Electronic supplementary information

Analysis and prediction of anion- and temperature responsive behaviours of luminescent Ru(II)-terpyridine complexes by using Boolean, fuzzy logic, artificial neural network and adapted neuro fuzzy inference models

Sourav Deb, Anik Sahoo, Priyam Mondal and Sujoy Baitalik[*]

Inorganic Chemistry Section, Department of Chemistry, Jadavpur University

Kolkata 700 032, India

Experimental section

Materials

Chemicals and solvents were purchased from local suppliers. 4-formyl-2,2':6',2''-terpyridine (tpy-PhCHO)[S1] and 2,6-bis(benzimidazole-2-yl)pyridine (H$_2$pbbzim) were prepared following reported procedures.[S2] [(tpy-PhCH$_3$)RuCl$_3$] and [(H$_2$pbbzim)RuCl$_3$] were synthesized by treating RuCl$_3$·3H$_2$O with tpy-PhCH$_3$ and H$_2$pbbzim, respectively in 1:1 molar ratio in refluxing EtOH.

Synthesis of the ligand

[(tpy-HImzPh$_3$(NMe$_2$)$_2$]

N,N dimethylbenzil (1.5 g, 2.45 mmol), tpy-PhCHO (0.825g 2.45mmol) and NH$_4$OAc (2.3 g, 30 mmol) were dissolved in CH$_3$COOH (10 mL) and refluxed for 3h. After cool down to RT, the resulting solution was poured into crushed ice (300 mL) and upon stirring, a yellowish compound that deposited was filtered. The resulting solid was filtered and thoroughly washed with water. Purification of the compound was performed through column chromatography using CHCl$_3$ as the eluting solvent and finally through recrystallization from CHCl$_3$-MeOH (1:1) mixture Yield, 1.1 g, (73%). ^{1}H NMR (400 MHz, DMSO-d_6, δ/ppm): 12.25 (s, 1H, NH (imidazole)), 8.75(s, 4H, 2H$_{3'}$+2H$_6$), 8.67(d, 2H, J=10.8 Hz, H$_3$), 8.26(d, 2H, J=11.6 Hz, H$_8$), 8.00-8.06 (m, 2H, H$_7$), 7.50-7.54(m, 2H, H$_4$), 7.38(d, 6H, J=11.6 Hz, H$_5$+H$_9$), 6.71 (d, 4H, J=12 Hz, H$_{10}$), 2.48(s,12H, Me). ESI-MS: m/z 614.34 ([L+H]$^+$). Anal. Calcd for C$_{40}$H$_{35}$N$_7$: C, 78.28; H, 5.75; N, 15.97. Found: C, 78.05; H, 5.82; N, 12.75.

Synthesis of metal complexes

[(tpy-PhCH$_3$)Ru(tpy-HImzPh$_3$(NMe$_2$)$_2$)](ClO$_4$)$_2$·H$_2$O (1)

Ru(tpy-PhCH$_3$)Cl$_3$ (80 mg, 0.15 mmol) and tpy-HImzPh$_3$(NMe$_2$)$_2$ (92 mg, 0.15 mmol) were added to 10 mL ethylene glycol and refluxed for 2h under Ar protection. The resulting solution was cooled to RT and upon spilling into an aqueous solution of NaClO$_4$ a red compound deposited. The compound was collected and purified by silica-gel column chromatography eluting with CH$_3$CN. Recrystallization from CH$_3$CN-MeOH (1:1, v/v) mixture results in the formation of a red microcrystalline compound. Yield: 97 mg (52%). ^{1}H NMR (400 MHz, DMSO-d_6, δ/ppm): 12.48(s, 1H, NH(imidazole)), 9.51(s, 2H, 2H$_{3'}$), 9.44(s, 2H, H$_{3''}$), 9.09(d, 4H, J=10.8 Hz, H$_6$+H$_{6'}$), 8.53(d, 2H, J=6.8 Hz, H$_8$), 8.35(d, 2H, J=10.8 Hz, H$_7$), 8.27(d, 2H, J=11.6

Hz, $H_{8'}$), 8.01-8.08(m, 4H, $H_4+H_{4'}$), 7.51-7.58 (m, 10H, $H_3+H_{3'}+H_7+H_9$), 7.24-2.30 (m, 4H, $H_5+H_{5'}$), 6.90(d, 4H, J=10.8 Hz, H_{10}), 2.48(s, 12H, Me(tpy-HimzPh3(NMe$_2$)), 2.35(s, 3H, Me(tpy-PhMe)). ESI-MS (positive, CH$_3$CN) m/z = 519.21 (100 %) [(tpy-PhCH$_3$) Ru (tpy-HImzPh$_3$(NMe$_2$)$_2$)]$^{2+}$. Anal. Calcd. for C$_{62}$H$_{54}$N$_{10}$Cl$_2$O$_9$Ru: C, 59.33; H, 4.34; N, 11.16. Found: C, 59.11; H, 4.21; N,11.02.

[Ru(tpy-HImzPh$_3$(NMe$_2$)$_2$)$_2$](ClO$_4$)$_2$·2H$_2$O (2)

Synthetic protocol for **2** is basically similar to that of **1**. In this case Ru(DMSO)$_4$Cl$_2$ (72 mg, 0.15 mmol) and tpy-HImzPh$_3$Me$_2$ (184 mg, 0.30 mmol) were taken in 1:2 molar ratio in ethylene glycol and refluxed for 3h. The compound was purified successively by silica gel column chromatography as well as recrystallization from MeCN-MeOH (1:1, v/v) in weakly acidic condition Yield: 94 mg (40%). ^{1}H NMR (400 MHz, DMSO-d_6, δ/ppm): 12.71(s, 1H, NH(imidazole)), 9.75(s, 4H, $H_{3'}$), 9.10 (d, 4H, J=8.0 Hz H_6), 8.70(d, 4H, J=11.6 Hz, H_8), 8.63(d, 4H, J=8.0 Hz, H_7), 8.07(t, 4H, J=10.0 Hz, H_4), 7.52(d, 4H, J=8.0 Hz, H_3), 7.47(d, 4H, J=8.0 Hz, H_9), 7.23 (t, 4H, J=10.6 Hz, H_5), 6.86 (d, 8H, J=12.0 Hz, H_{10}), 2.48 (s, 24H, Me(tpy-HimzPh$_3$NMe$_2$)).ESI-MS(positive,CH$_3$CN)m/z = 664.25 (100%) [Ru(tpy-HImzPh$_3$ (NMe$_2$)$_2$)$_2$]$^{2+}$. Anal. Calcd. for C$_{80}$H$_{74}$N$_{14}$Cl$_2$O$_{10}$Ru: C, 61.46; H, 4.77; N, 12.54. Found: C, 61.11; H, 4.23; N,12.75.

[(H$_2$pbbzim) Ru(tpy-HImzPh$_3$(NMe$_2$)$_2$)](ClO$_4$)$_2$·H$_2$O (3)

Complex **3** was prepared by following the same procedure as **1**. In this case [(H$_2$pbbzim)RuCl$_3$] (78 mg, 0.15 mmol) was used in place of Ru(tpy-PhCH$_3$)Cl$_3$ and recrystallization was carried out in CH$_3$CN-H$_2$O (2:1, v/v) mixture under weakly acidic condition. Yield: 90 mg (48%). ^{1}H NMR (400 MHz, DMSO-d_6, δ/ppm): 15.0(s, 1H, NH(Py2,6)), 12.85(s, 1H, NH(imidazole)), 9.62(s, 2H, $H_{3'}$), 8.86(d, 2H, J=10.8 Hz, H_6), 8.71(d, 2H, J=11.2 Hz, H_8), 8.65-8.62(m, 2H, H_{15}), 8.50-8.47(m, 1H, H_{16}), 8.38(d, 2H, J=11.6 Hz, H_7), 7.89-7.86(m, 2H, H_4), 7.61(d, 2H, J=10.8 Hz, H_{14}), 7.41(d, 6H, J=11.8 Hz, H_3+H_9), 7.25-7.24(m, 4H, H_5+H_{13}), 7.0 (t, 2H, J=10.4 Hz, H_{12}), 6.70(d, 4H, J=11.2 Hz, H_{10}), 6.05(d, 2H, J=10.8 Hz, H_{11}), 2.48(s, 12H, Me). ESI-MS (positive, CH$_3$CN) m/z = 513.21 (100 %) [(H$_2$pbbzim)Ru(tpy-HImzPh$_3$(NMe$_2$)$_2$]$^{2+}$. Anal. Calcd. for C$_{59}$H$_{50}$N$_{12}$Cl$_2$O$_9$Ru: C, 57.01; H, 4.05; N, 13.52. Found: C, 56.61; H, 3.83; N,13.85

Caution! Perchlorate salts of the metal complexes are explosive and should be handled in small amount with extreme care

Characterization

Fig S1-S4 (ESI) display the ESI mass spectra of tpy-HImzPh$_3$(NMe$_2$)$_2$ and the complexes (**1-3**) in MeCN. The agreement among the simulated and experimental isotopic distribution is quite good. The abundant peak appears in the domain of 513.21-664.25 m/z and corresponds to di-positive cation of the complexes. ^{1}H NMR spectra of tpy-HImzPh$_3$(NMe$_2$)$_2$ and the complexes are displayed in Fig. S5. All the peaks are tentatively assigned by using their ^{1}H-^{1}H COSY NMR spectra and by comparing the spectra of the structurally similar derivatives.[S3-S4] All the complexes display a sharp peak at 2.48 ppm corresponding to their NMe$_2$ protons (12 for both **1** and **3** and 24 for **2**). **1** shows a singlet at 2.35 ppm integrating 3 protons due to -CH$_3$ unit in tpy-PhCH$_3$ moiety. The doublet at 6.05 ppm for **3** corresponds to H$_{11}$ in H$_2$pbbzim motif. **1** and **2** displays one broad singlet at ~12.5 ppm due to imidazole NH proton, while **3** exhibits two NH resonances of unequal intensity at 12.85 and 15.00 ppm due to two types of NH protons. The peak at 12.85 ppm is due to NH of tpy-HImzPh$_3$(NMe$_2$)$_2$, whereas the signal at 15.00 ppm with double intensity corresponds to NH of H$_2$pbbzim. H$_{3'}$, H$_6$, H$_7$ and H$_8$ protons underwent a down-field shift, whereas the phenyl protons and H$_4$ of tpy-unit remain almost unaltered upon coordination to Ru^{2+}. H$_3$ of tpy unit underwent a remarkable up-field shift as it is underneath the ring current of a pyridine ring of another tpy ligand.

Physical measurements

Elemental analyses of the compounds were performed with a Vario-Micro V2.0.11 elemental (CHNSO) analyzer. NMR spectra were collected on a Bruker 400 MHz spectrometer in DMSO-d_6 for both the ligand and metal complexes. High resolution mass spectroscopy was performed on a Waters Xevo G2 QTOf mass spectrometer. The UV-vis absorption spectra were recorded with a Shimadzu UV 1800 spectrometer. Steady state luminescence spectra were obtained by a Horiba Fluoromax-4 spectrometer. Luminescence quantum yields were determined by using literature method taking [Ru(bpy)$_3$]$^{2+}$ as the standard. Luminescence lifetime measurements were carried out by using time–correlated single photon counting set up from Horiba Jobin-Yvon. The

luminescence decay data were collected on a Hamamatsu MCP photomultiplier (R3809) and were analyzed by using EZ time software.

Experimental uncertainties are as follows: absorption maxima, ± 2 nm; molar absorption coefficients, 10%; emission maxima, ± 5 nm; excited–state lifetimes, 10%; luminescence quantum yields, 20%.

The binding/equilibrium constants were evaluated from absorption/emission titration data using equation (S1).[S5,S6]

$$\Delta A = \frac{\Delta\varepsilon b([H] + [G] + (1/K)) \pm \sqrt{\Delta\varepsilon^2 b^2 ([H] + [G] + (1/K))^2 - 4\Delta\varepsilon^2 b^2 [H][G]}}{2} \tag{S1}$$

where ΔA is the change in absorbance, [H] and [G] is the concentration of metal complex and added anion, respectively. $\Delta\varepsilon$ is the change in molar extinction coefficient, b is the absorption path length, and K is the binding constant. Non-linear regression analysis of absorption/emission spectral data as a function of anion concentration lead to the value of binding constants. Binding constants were performed in duplicate, and the average value is reported.

Detection limits of complexes were determined by utilizing their absorption/emission titration profiles. The curves plotted between normalized absorbance or luminescence intensity *vs*. Log[anion] are shown in Fig. S21-S32. Linear regression curves as fitted to the intermediate values are also shown in the said figures. The point at which the line crossed the ordinate axis was taken as the detection limit of the anion.

Artificial neural networks (ANNs)

An artificial neural network is a network stimulated by the central nervous system of the animals, primarily the brain. ANNs are often employed to guess functions which could rely on huge number of unknown inputs. Among the two principal categories of neural networks, viz. recurrent (RNN) and feed-forward (FFN), we employed FNN in the present study due to static nature of our system. FNN is the simplest and convenient category of network where the information passes into a particular direction, proceeds, from the input nodes, via the hidden notes, and finally to the output nodes. Additionally, due to its high efficiency in forecasting static system, we implemented advanced feed-forward back propagation network, namely, ANN-function fitting (ANN-FF) network for deeper understanding and forecasting of the system.

Artificial neural network model consisting of 2 inputs, 5 hidden layers and 1 output. In ANN-FF, the relation between the input and output is assumed to be a function, which is approximated using the experimental data. The network diagram of the ANN-FF for the system can be found in Fig. S36. It can fit multidimensional mapping problems arbitrarily well when consistent data and enough neurons are designed in the hidden layer. For function fitting of the problem, a neural network is needed to map between a data set of numeric inputs and a set of numeric targets. Hence, each pattern is assigned a number (e.g., 1, 2, 3, 4, etc.).

In this study, a neural network for function fitting was coded in MATLAB 2018. The input data present the network, while the target data define the desired network output. Table S6 represents the emission intensity outputs upon the action of 40 different combinations of two inputs (input 1=H^+ and input 2=F^-). Thus, the 40×2 matrix represents the static input data of 40 samples involving 2 inputs, while 40×1 matrix represents the static output data (at 678 nm) of one element. Now, the 40 samples are divided into 3 sets of data. 70% of the data are conferred for the training and the network is corrected according to its error. Now the learning algorithm and the number of neurons in the hidden layer were optimized. 15% data are employed to compute the network generalization and to halt training. When generalization stops improving, the data validation takes place. The remaining 15% data give an independent estimate of the network performance during and after the training, called testing data (Fig. 9a)

Adaptive neuro-fuzzy inference system (ANFIS)

The network framework of the ANFIS is illustrated in Fig. S37. It consists of five connected layers (excluding input layer) which is common for the two input dimensions, P and Q, both of which possess three fuzzy sets, viz. C1C2C3 for P, while D1D2D3 for Q input. We have chosen A number of inputs and B number of fuzzy set to represent each input which in turn implies A×B number of nodes in Layer 1. In Layer 2, all the nodes are interconnected with the membership function output of each input node, yielding a total of B^A node in Layer 2. Layer 3 and 4 possess the same number of nodes as that of Layer 2. Layer 5, on the other hand, possess only one node representing the output of the network. Upon considering each input as a node, the total number of nodes in the architecture will be A + A×B + 3×B^A + 1. In ANFIS, only the membership function parameters in Layer 1 and inputs weight in Layer 4 are to be predicted by training. Upon implication of the triangular membership function (*trimf*) which is represented by

three parameters, we need to assess 3×B×A premise parameters in Layer 1 and A×B^A consequent weight parameters in Layer 4.

The structure of the ANFIS is automatically tuned by least-squares estimation and the back-propagation algorithm. A fuzzy set A of a universe of discourse X is represented by a collection of ordered pairs of generic elements and its membership function $\mu_A(x)$: X tends to [0 1], which associates a number $\mu A(x)$ to each element x of X. The fuzzy logic controller works on the basis of a set of control rules (called the fuzzy rules) among the linguistic variables. These fuzzy rules are represented in the form of conditional statements.

The basic structure of the pattern predictor model developed using ANFIS to predict the pattern of the flow regime consists of four important parts, namely, the fuzzification, knowledge base, artificial neural network, and defuzzification blocks, as shown in Scheme 1. The inputs to the ANFIS are the H^+ and F^-. These are fed to the fuzzification unit, which converts the binary data into linguistic variables. These in turn are given as inputs to the knowledge base block. The ANFIS tool in MATLAB 2018 developed 49 rules while training the neural network. The knowledge base block is connected to the artificial neural network block. A hybrid optimization algorithm is used to train the neural network and to select the proper set of rules for the knowledge base. To predict the emission intensity values at 678 nm, training is an important step in the selection of the proper rule base. Once the proper rule base is selected, the ANFIS model is ready to carry out prediction. The trained ANFIS was validated using 15% of the data. The output of the artificial neural network unit is given as input to the defuzzification unit, where the linguistic variables are converted back into numerical data in crisp form.

Tables for electronic supplementary information

Table S1 Photophysical parameters of the complexes in various solvents

Compounds		Absorption λ$_{max}$/ nm (ε,M^{-1}cm^{-1})	Luminescence		
			λ$_{max}$/ nm	τ/ns	Φ
1	MeCN(298K)	492(37100),327(sh)(62600),308(84600), 285(71800)	662	τ$_1$=1.6(15%) τ$_2$=6.0(85%)	1.2×10^{-3}
2		494(39000),330(sh) (73000),310(91800), 287(83200)	658	τ$_1$=1.2(6%) τ$_2$=5.5(94%)	0.9×10^{-3}
3		488(45300),345(82400), 328 (91300), 310(103900),284(81200),240(76400)	678	τ=28	2.5×10^{-3}
1	DMSO(298K)	503(38500),330(sh)(66900),315(82900), 290(69800)	670	τ$_1$=3.3(16%) τ$_2$=10.7(84%)	1.1×10^{-3}
2		508(33400),332(sh) (60400),314(72800), 288(67100)	665	τ$_1$=1.6(20%) τ$_2$=10.0(80%)	1.2×10^{-3}
3		508(35900),346(sh)(73700),314(99400), 285(85200)	696	τ=102	3.2×10^{-3}
1	Water (298K)	495(42300),327(sh)(75700),310(97500), 285(87200)	660	τ$_1$=0.5(25%) τ$_2$=9.0(75%)	0.7×10^{-3}
2		498(42500),328(sh)(81300),310(102800) ,286(98300)	658	τ$_1$=0.5(11%) τ$_2$=10.0(89%)	0.5×10^{-3}
3		512(40700),347(79300),316(109500), 285(94200)	683	τ$_1$=10(12%) τ$_2$=50(88%)	2.1×10^{-3}
1	EtOH-MeOH (4:1),(77K)		633	τ=18.6 μs	0.22
2			638	τ=18.0 μs	0.25
3			664	τ=12.0μs	0.32

Table S2 Non linear fitting parameters of temperature dependent experiment of the complexes (**1-3**) in MeCN

Complex	k_1/s^{-1}	k_2/s^{-1}	ΔE_2/cm^{-1}
1	5.9×10^4	2.2×10^{13}	3574±25
2	5.5×10^4	2.6×10^{13}	3731±25
3	8.3×10^4	2.0×10^{13}	3876±72

Table S3 Value of binding constants [a,b] (K) for **1-3** in MeCN and H_2O at RT

Anions	1		2		3	
From Absorption spectra (acetonitrile medium)						
	K_1	K_2	K_1	K_2	K_1	K_2
F^-	1.7×10^5	-	2.6×10^5	3.1×10^4	1.4×10^5	1.2×10^4
From Absorption spectra (aqueous medium)						
CN^-	3.5×10^4		2.8×10^4	-	3.4×10^4	4.5×10^3
From Emission spectra (acetonitrile medium)						
Anions	1		2		3	
	K_1	K_2	K_1	K_2	K_1	K_2
F^-	1.6×10^5	-	1.5×10^5	1.8×10^4	1.6×10^5	2.3×10^4
From Emission spectra (aqueous medium)						
CN^-	3.0×10^4	-	3.8×10^4		3.7×10^4	3.7×10^3

[a]t-Butyl salts of the respective anions were used for the studies. [b]Estimated errors were < 15 %.

Table S4 Value of limit of detection of **1-3** in MeCN and H_2O

Compounds	Detection Limit (M) in acetonitrile medium		Detection Limit (M) in aqueous medium	
	F^-		CN^-	
	Absorption	Emission	Absorption	Emission
1	2.3×10^{-8}	4.0×10^{-8}	7.5×10^{-8}	7.3×10^{-8}
2	6.3×10^{-8}	8.0×10^{-8}	7.9×10^{-8}	8.0×10^{-8}
3	4.0×10^{-8}	9.5×10^{-8}	7.5×10^{-8}	7.8×10^{-8}

Table S5 Rules for the fuzzy logic system by taking H^+ (input 1) and F^- (input 2) as the inputs and emission intensity at 678 nm as the outputs For **3**. The rules comprise of the following statements

```
1. If (input1 is L) and (input2 is L) then (output1 is H) (1)
2. If (input1 is L) and (input2 is M) then (output1 is H) (1)
3. If (input1 is L) and (input2 is H) then (output1 is H) (1)
4. If (input1 is M) and (input2 is L) then (output1 is H) (1)
5. If (input1 is M) and (input2 is M) then (output1 is M) (1)
6. If (input1 is M) and (input2 is H) then (output1 is H) (1)
7. If (input1 is H) and (input2 is L) then (output1 is L) (1)
8. If (input1 is H) and (input2 is M) then (output1 is M) (1)
9. If (input1 is H) and (input2 is H) then (output1 is M) (1)
10. If (input1 is L) then (output1 is H) (1)
11. If (input1 is M) then (output1 is M) (1)
12. If (input1 is H) then (output1 is L) (1)
13. If (input2 is L) then (output1 is H) (1)
14. If (input2 is M) then (output1 is H) (1)
15. If (input2 is H) then (output1 is H) (1)
```

Table S6 Different values of emission intensity as a function of n_H^+/n_1 and n_F^-/n_1 for **3**

No of obs.	Equiv. of H^+	Equiv. of F^-	Emission Intensity at 678nm
1	0.0	0.0	92.00
2	4.0	0.0	1.34
3	0.0	5.0	92.05
4	0.5	2.5	75.32
5	2.5	1.5	40.00
6	2.0	2.5	42.00
7	4.0	1.5	26.30
8	2.0	2.0	41.00
9	1.5	1.0	64.00
10	3.5	5.0	39.33
11	2.5	3.5	47.00
12	0.5	4.0	86.78
13	3.5	4.5	37.89
14	1.0	3.0	74.34
15	1.5	5.0	84.23
16	2.5	4.5	48.45
17	2.0	4.0	52.34
18	1.0	5.0	82.15
19	1.5	5.0	83.24
20	4.0	1.0	24.76
21	3.0	4.0	37.05
22	0.5	3.5	84.67
23	1.0	1.5	72.78
24	1.5	4.5	46.78
25	2.5	4.0	38.90
26	3.0	4.5	39.65
27	3.5	5.0	38.95
28	2.0	5.0	56.46
29	1.5	1.5	66.76
30	2.0	3.0	48.76
31	3.5	2.5	28.76
32	3.0	1.0	17.30
33	2.0	3.5	50.32
34	1.0	4.5	90.10
35	0.5	3.0	78.56
36	1.5	3.5	41.23
37	2.5	3.0	32.45
38	4.0	2.5	26.78
39	2.0	2.5	44.56
40	1.0	3.5	76.89

Table S7 Rules for the ANFIS (based on Sugeno's method) by taking H^+ as input 1 and F^- as input 2, whereas emission intensity at 678nm as the output. The rules comprise of the following statements

```
1. If (input1 is in1mf1) and (input2 is in2mf1) then (output is out1mf1) (1)
2. If (input1 is in1mf1) and (input2 is in2mf2) then (output is out1mf2) (1)
3. If (input1 is in1mf1) and (input2 is in2mf3) then (output is out1mf3) (1)
4. If (input1 is in1mf1) and (input2 is in2mf4) then (output is out1mf4) (1)
5. If (input1 is in1mf1) and (input2 is in2mf5) then (output is out1mf5) (1)
6. If (input1 is in1mf1) and (input2 is in2mf6) then (output is out1mf6) (1)
7. If (input1 is in1mf1) and (input2 is in2mf7) then (output is out1mf7) (1)
8. If (input1 is in1mf2) and (input2 is in2mf1) then (output is out1mf8) (1)
9. If (input1 is in1mf2) and (input2 is in2mf2) then (output is out1mf9) (1)
10. If (input1 is in1mf2) and (input2 is in2mf3) then (output is out1mf10) (1)
11. If (input1 is in1mf2) and (input2 is in2mf4) then (output is out1mf11) (1)
12. If (input1 is in1mf2) and (input2 is in2mf5) then (output is out1mf12) (1)
13. If (input1 is in1mf2) and (input2 is in2mf6) then (output is out1mf13) (1)
14. If (input1 is in1mf2) and (input2 is in2mf7) then (output is out1mf14) (1)
15. If (input1 is in1mf3) and (input2 is in2mf1) then (output is out1mf15) (1)
16. If (input1 is in1mf3) and (input2 is in2mf2) then (output is out1mf16) (1)
17. If (input1 is in1mf3) and (input2 is in2mf3) then (output is out1mf17) (1)
18. If (input1 is in1mf3) and (input2 is in2mf4) then (output is out1mf18) (1)
19. If (input1 is in1mf3) and (input2 is in2mf5) then (output is out1mf19) (1)
20. If (input1 is in1mf3) and (input2 is in2mf6) then (output is out1mf20) (1)
21. If (input1 is in1mf3) and (input2 is in2mf7) then (output is out1mf21) (1)
22. If (input1 is in1mf4) and (input2 is in2mf1) then (output is out1mf22) (1)
23. If (input1 is in1mf4) and (input2 is in2mf2) then (output is out1mf23) (1)
24. If (input1 is in1mf4) and (input2 is in2mf3) then (output is out1mf24) (1)
25. If (input1 is in1mf4) and (input2 is in2mf4) then (output is out1mf25) (1)
26. If (input1 is in1mf4) and (input2 is in2mf5) then (output is out1mf26) (1)
27. If (input1 is in1mf4) and (input2 is in2mf6) then (output is out1mf27) (1)
28. If (input1 is in1mf4) and (input2 is in2mf7) then (output is out1mf28) (1)
29. If (input1 is in1mf5) and (input2 is in2mf1) then (output is out1mf29) (1)
30. If (input1 is in1mf5) and (input2 is in2mf2) then (output is out1mf30) (1)
31. If (input1 is in1mf5) and (input2 is in2mf3) then (output is out1mf31) (1)
32. If (input1 is in1mf5) and (input2 is in2mf4) then (output is out1mf32) (1)
33. If (input1 is in1mf5) and (input2 is in2mf5) then (output is out1mf33) (1)
34. If (input1 is in1mf5) and (input2 is in2mf6) then (output is out1mf34) (1)
35. If (input1 is in1mf5) and (input2 is in2mf7) then (output is out1mf35) (1)
36. If (input1 is in1mf6) and (input2 is in2mf1) then (output is out1mf36) (1)
37. If (input1 is in1mf6) and (input2 is in2mf2) then (output is out1mf37) (1)
38. If (input1 is in1mf6) and (input2 is in2mf3) then (output is out1mf38) (1)
39. If (input1 is in1mf6) and (input2 is in2mf4) then (output is out1mf39) (1)
40. If (input1 is in1mf6) and (input2 is in2mf5) then (output is out1mf40) (1)
41. If (input1 is in1mf6) and (input2 is in2mf6) then (output is out1mf41) (1)
42. If (input1 is in1mf6) and (input2 is in2mf7) then (output is out1mf42) (1)
43. If (input1 is in1mf7) and (input2 is in2mf1) then (output is out1mf43) (1)
44. If (input1 is in1mf7) and (input2 is in2mf2) then (output is out1mf44) (1)
45. If (input1 is in1mf7) and (input2 is in2mf3) then (output is out1mf45) (1)
46. If (input1 is in1mf7) and (input2 is in2mf4) then (output is out1mf46) (1)
47. If (input1 is in1mf7) and (input2 is in2mf5) then (output is out1mf47) (1)
48. If (input1 is in1mf7) and (input2 is in2mf6) then (output is out1mf48) (1)
49. If (input1 is in1mf7) and (input2 is in2mf7) then (output is out1mf49) (1)
```

Figures for electronic supplementary information
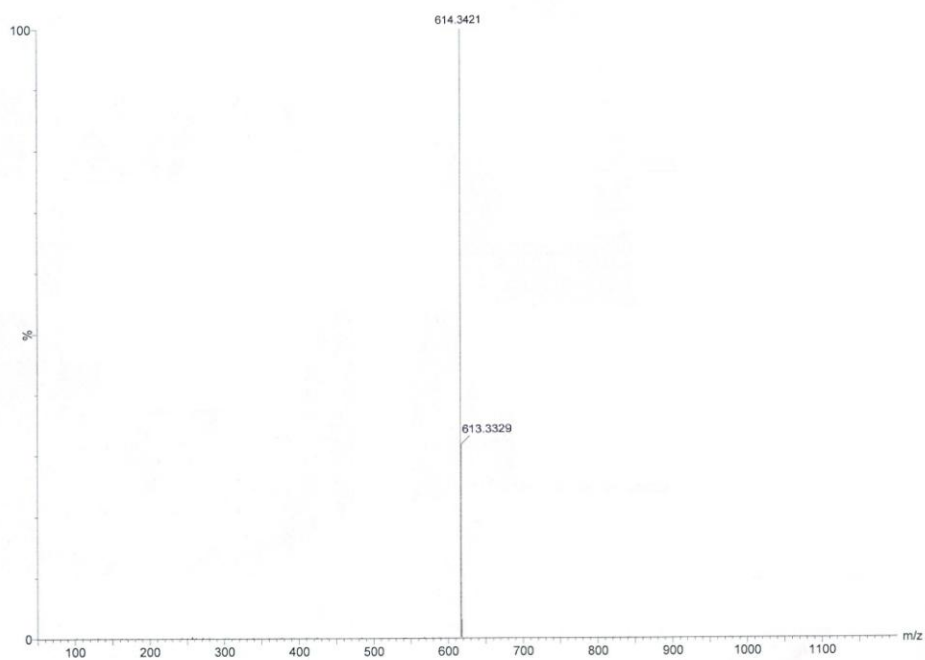
Fig. S1 ESI (positive) mass spectrum for tpy-HImzPh$_3$(NMe$_2$)$_2$ ligand. (m/z = 614.34) ([L+H]$^+$) in MeCN.
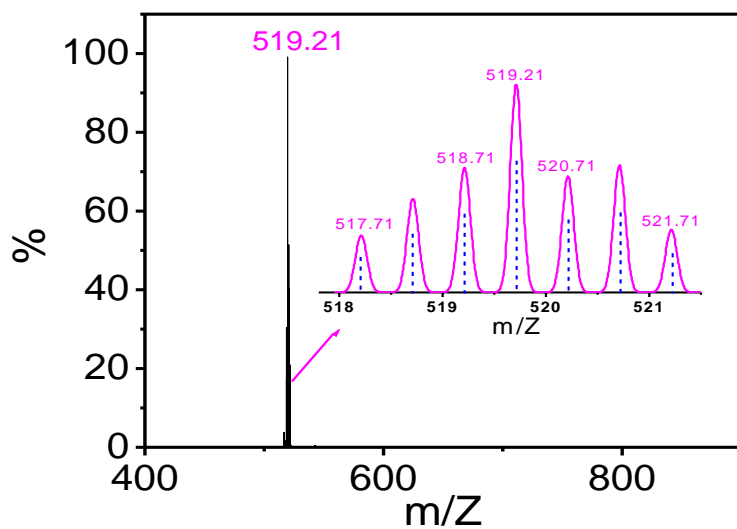
Fig. S2 ESI (positive) mass spectrum for the complex cation of **1** [(tpy-PhCH$_3$)Ru(tpy-HImzPh$_3$(NMe$_2$)$_2$]$^{2+}$ (m/z = 519.21) in MeCN showing both observed and simulated isotopic distribution patterns.
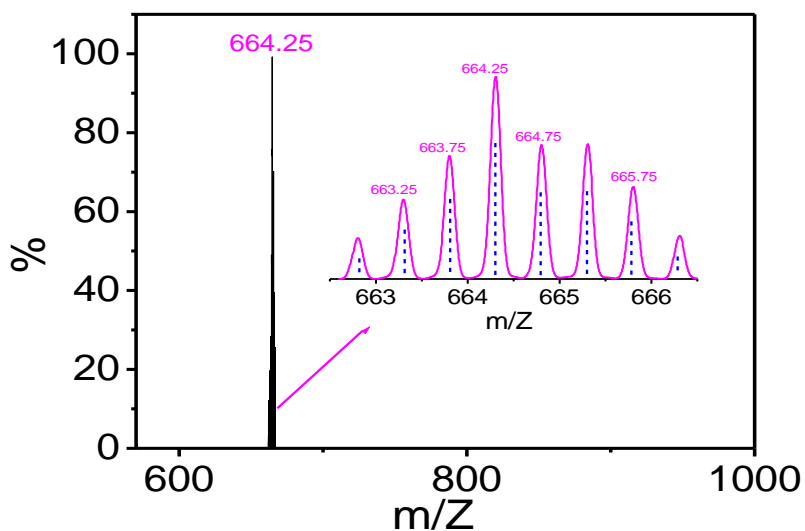

Fig. S3 ESI (positive) mass spectrum for the complex cation of **2** [Ru(tpy-HImzPh$_3$(NMe$_2$)$_2$)$_2$]$^{2+}$ (m/z = 664.25) in MeCN showing both observed and simulated isotopic distribution patterns.
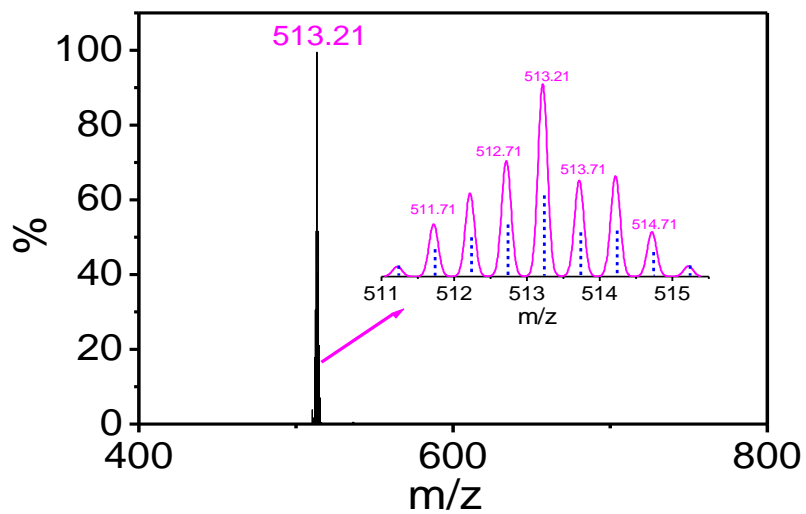
Fig. S4 ESI (positive) mass spectrum for the complex cation of **3** [(H$_2$pbbzim) Ru (tpy-HImzPh$_3$(NMe$_2$)$_2$]$^{2+}$ (m/z=513.21) in MeCN showing both observed and simulated isotopic distribution patterns.
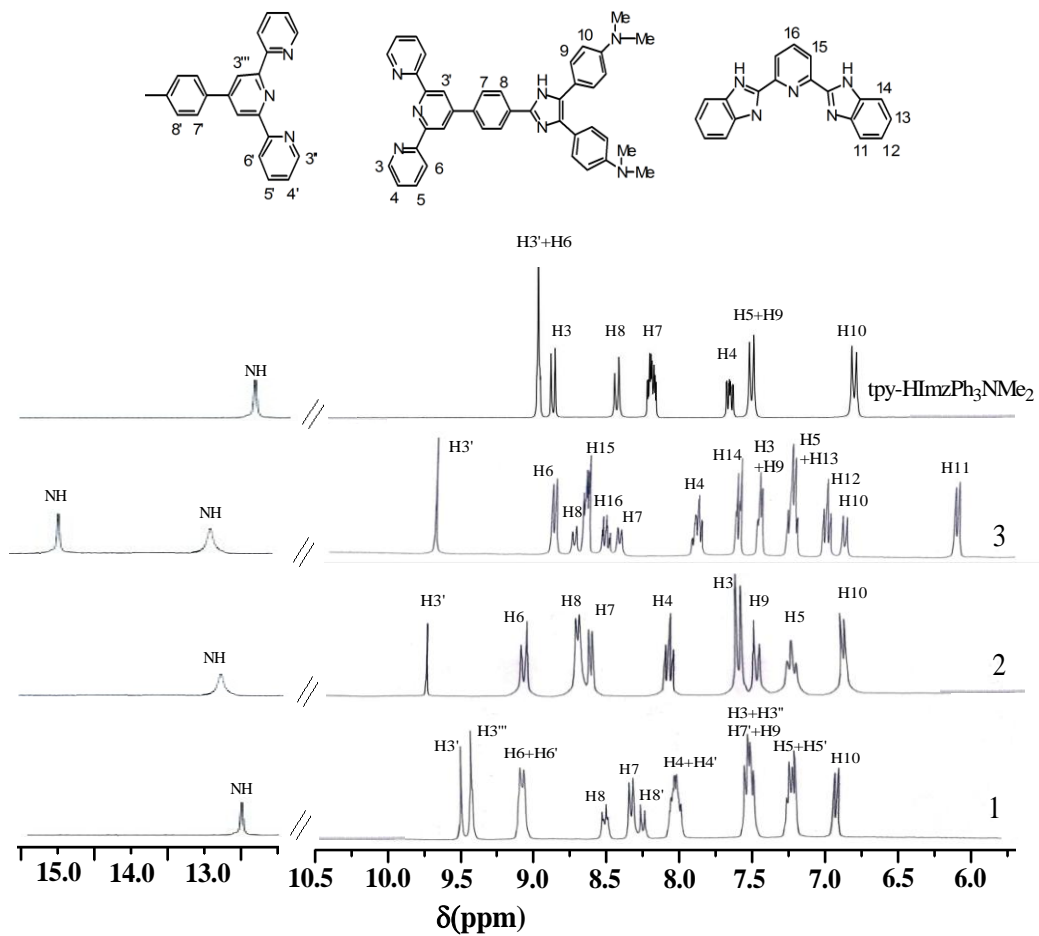
Fig. S5 ^{1}H NMR spectra of the complexes in DMSO-d_6.
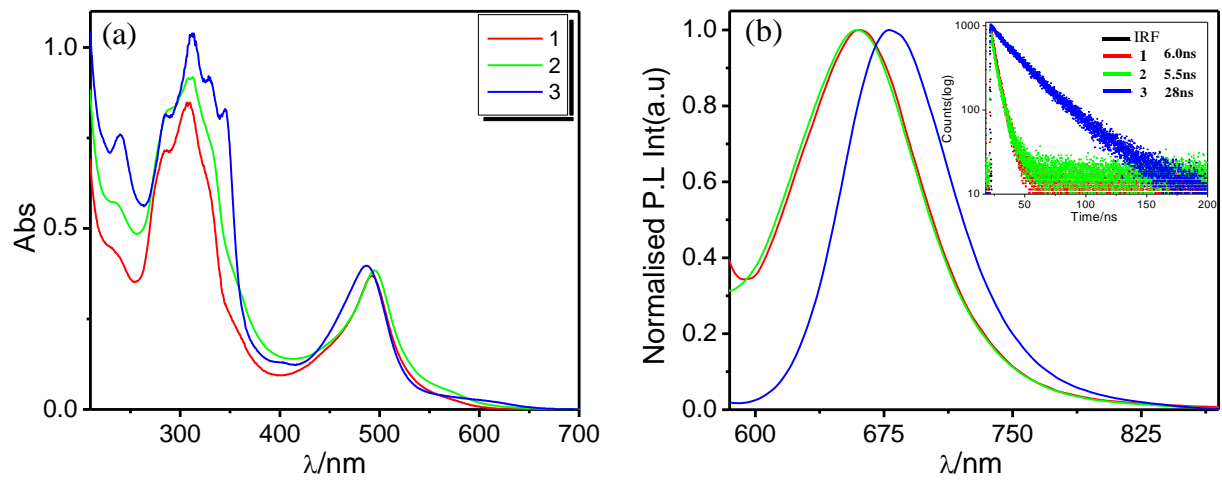
Fig. S6 Absorption (a) emission (b) (λ_{ex} = 490 nm) spectra of **1-3** in MeCN at RT. The decay profiles and corresponding lifetimes are presented in the inset of (b).
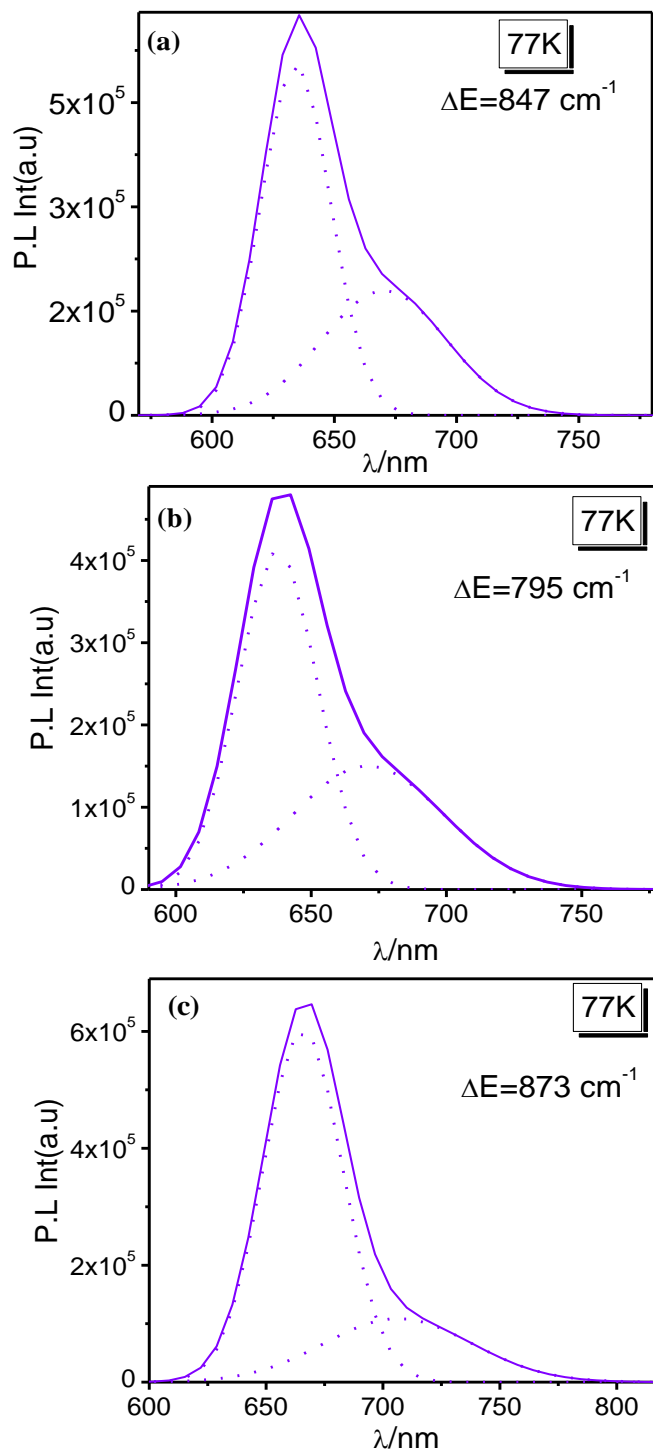
Fig. S7 Experimental (solid line) and deconvoluted (dotted line) emission spectra of **1** (a), **2** (b), and **3** (c) in EtOH-MeOH (4:1v/v) at 77 K. The insets show the values of vibrational spacing.
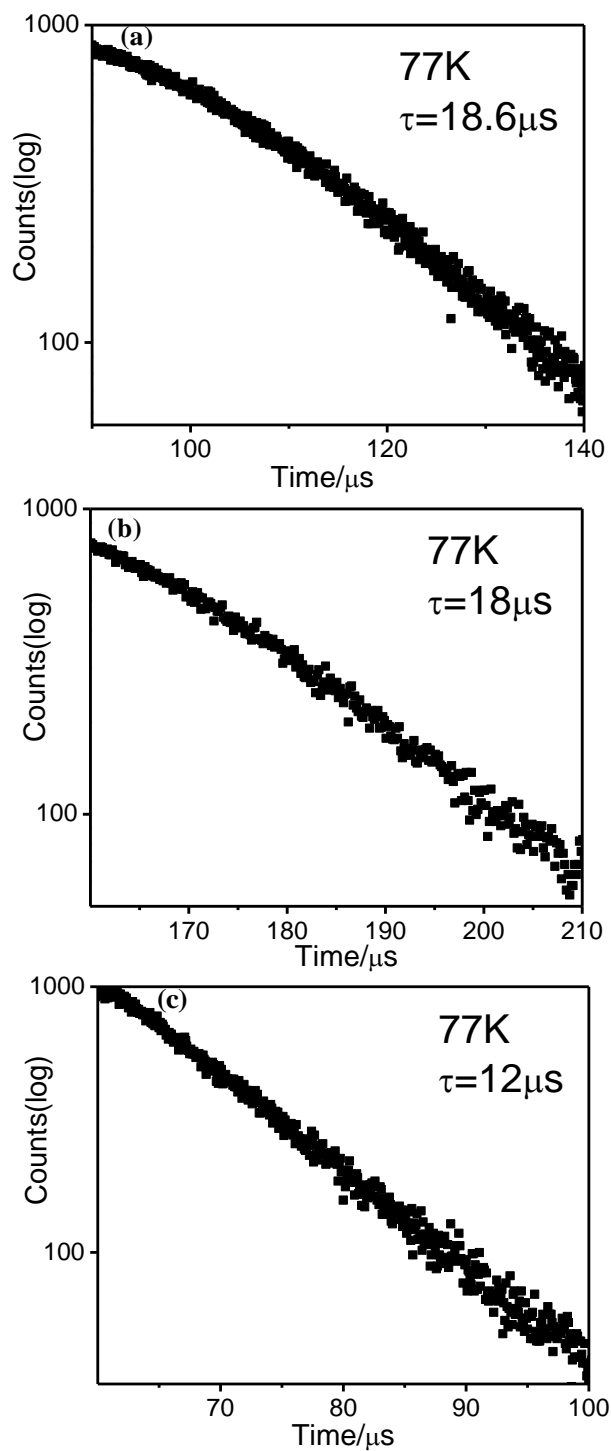
Fig. S8 Excited state decay profiles together with the lifetime of **1** (a), **2** (b), and **3** (c) in EtOH-MeOH (4:1, v/v) glass at 77 K in MCS mode.
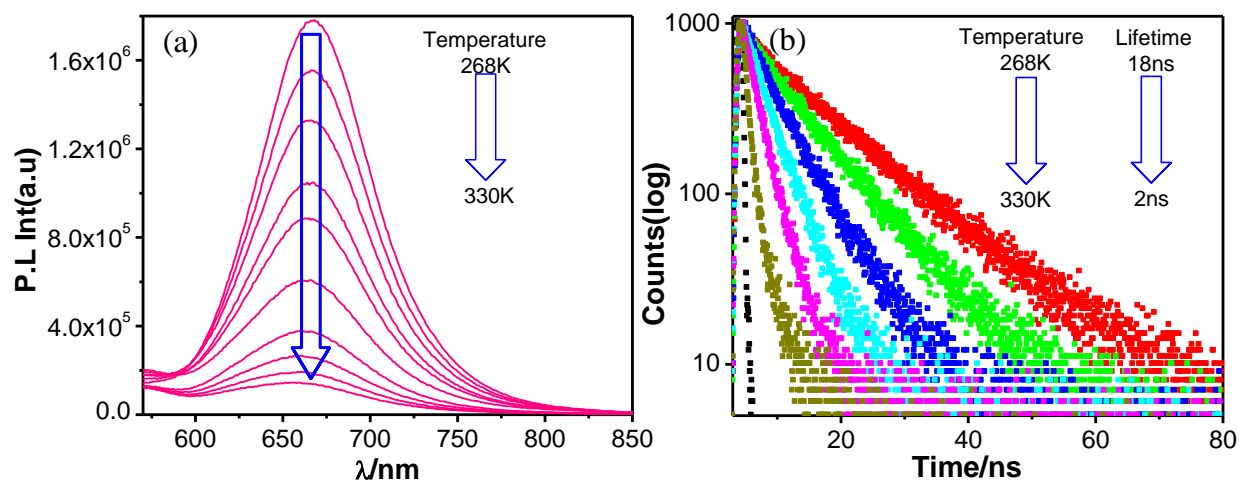
Fig. S9 Variation of luminescence spectrum (a) and excited state decay profile (b) of **1** in MeCN as a function of temperature (T).
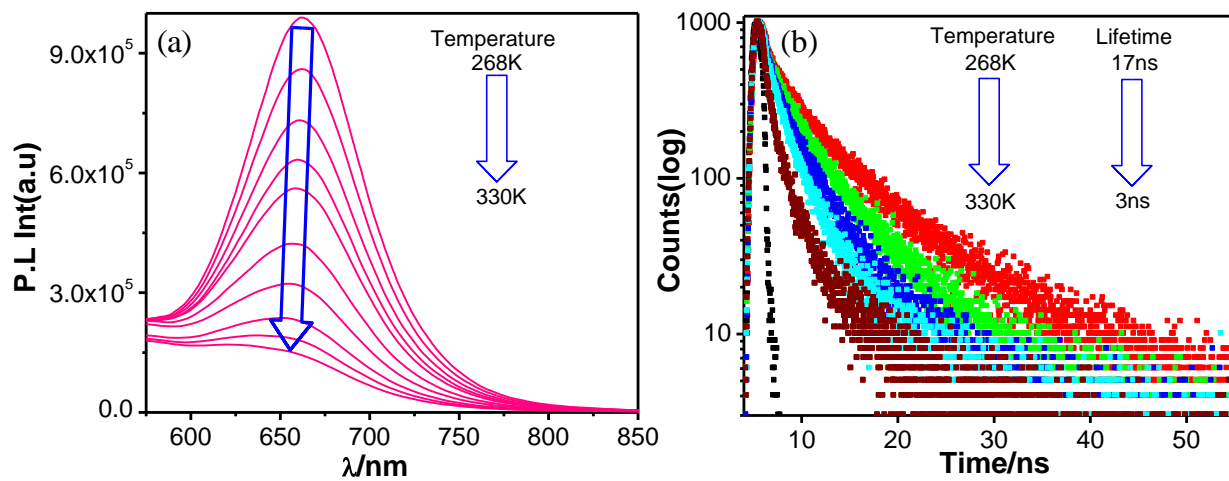
Fig. S10 Variation of luminescence spectrum (a) and excited state decay profile (b) of **2** in MeCN as a function of temperature (T).
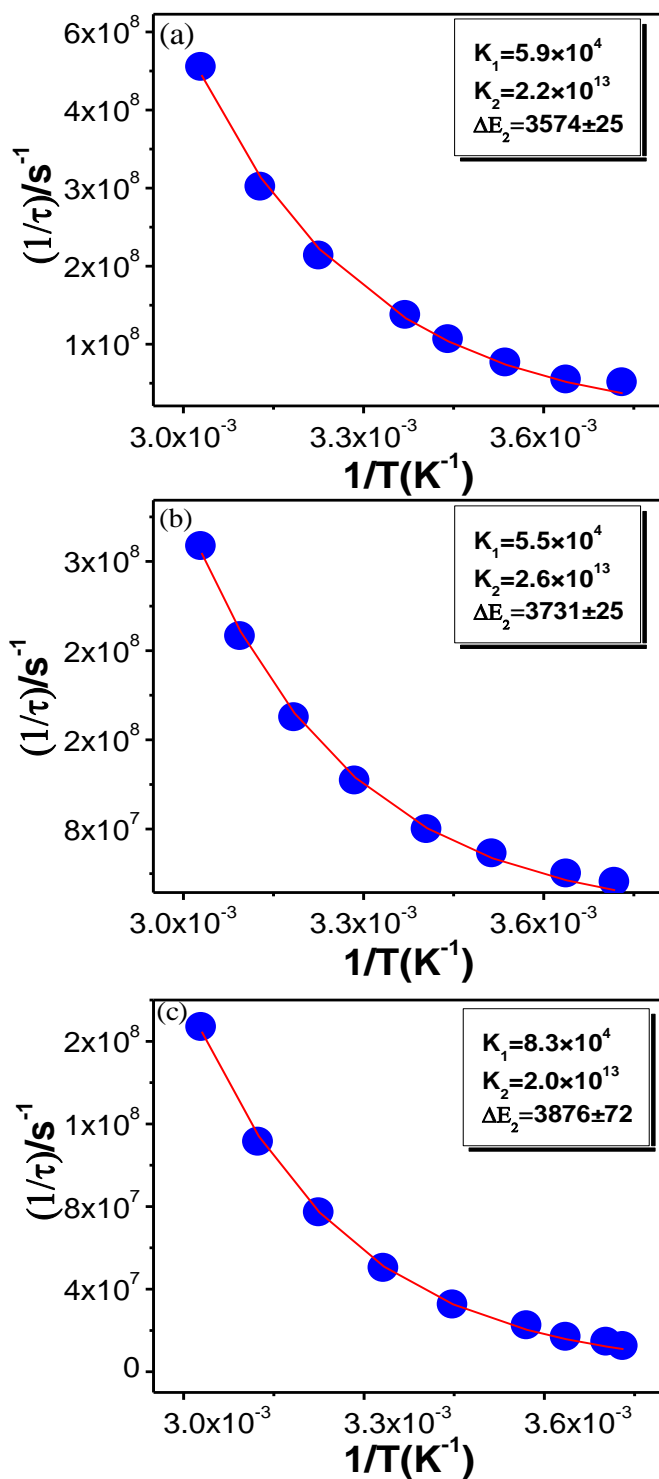
Fig. S11 Nonlinear fits of $1/\tau$ vs $1/T$ plot. Inset shows different temperature dependent parameters of the complexes of **1**(a), **2**(b) and **3**(c).
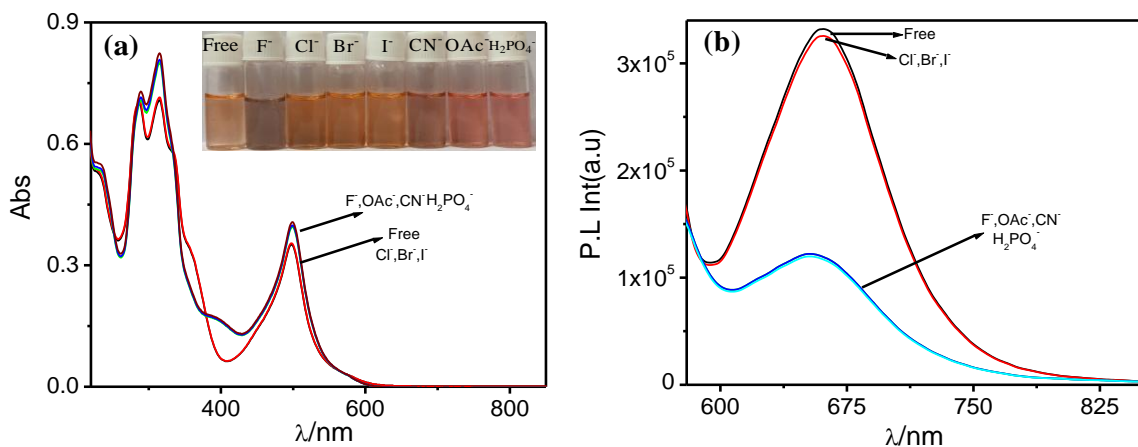
Fig. S12 Absorption and emission spectral profile of **1** in MeCN (a and b, respectively) as a function of various anions. Inset of (a) show the visual color changes.
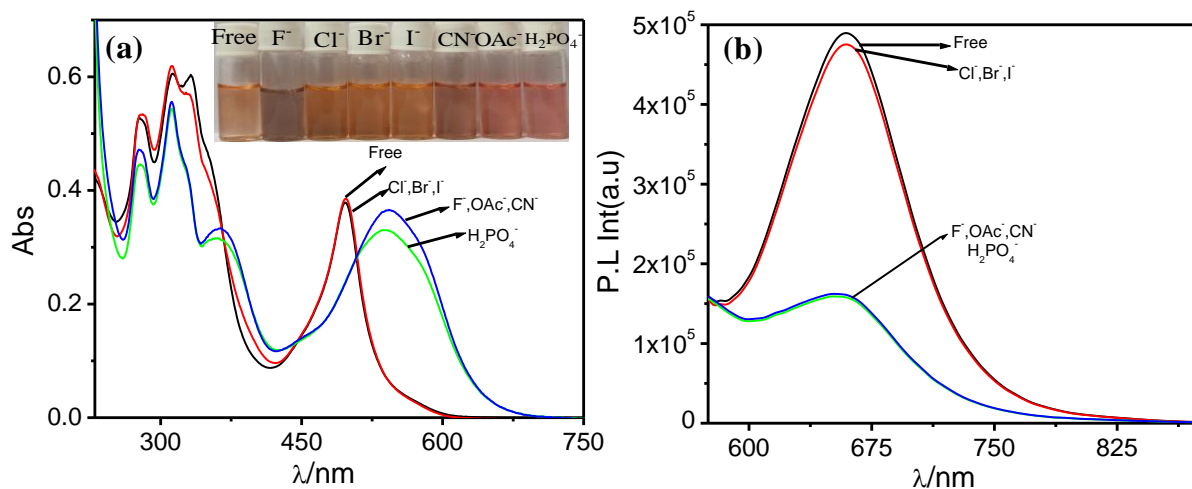
Fig. S13 Absorption and emission spectral profile of **2** in MeCN (a and b, respectively) as a function of various anions. Inset of (a) show the visual color changes.
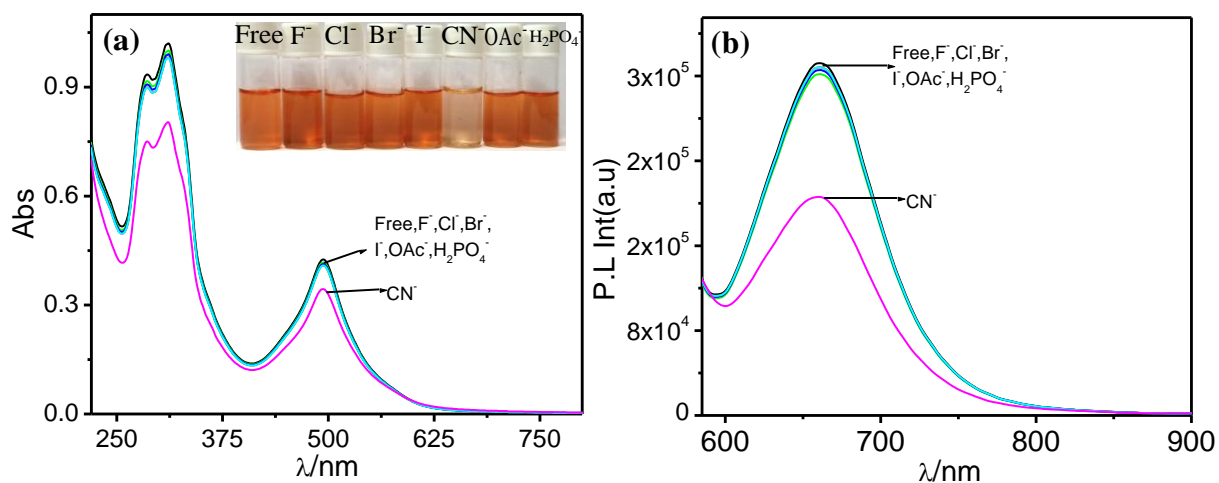
Fig. S14 Absorption and emission spectral profile of **1** in water-HEPES buffer (pH = 7.4) (a and b, respectively) as a function of various anions. Inset of (a) show the visual color changes.
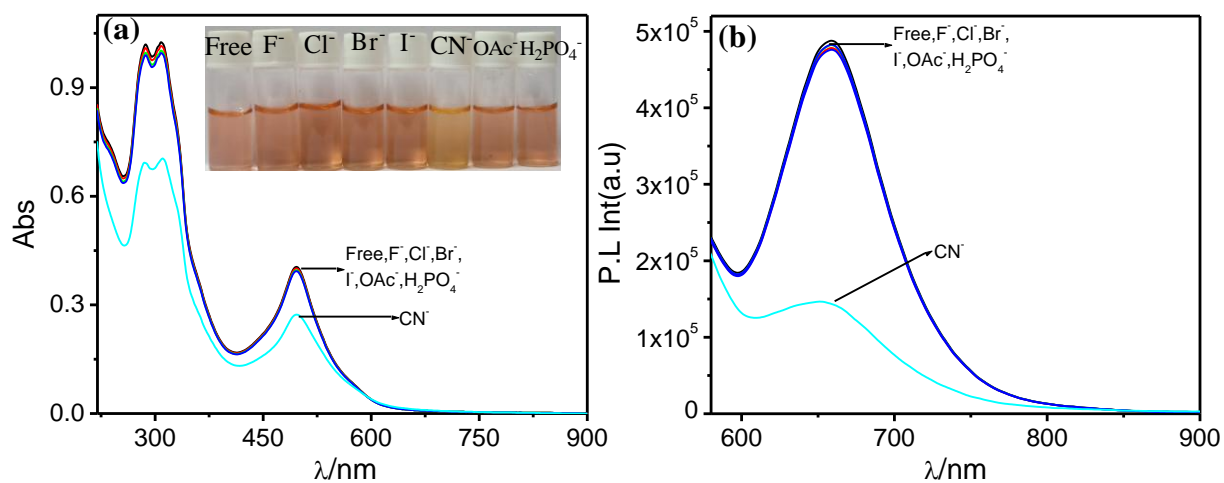
Fig. S15 Absorption and emission spectral profile of **2** in water-HEPES buffer (pH = 7.4) (a and b, respectively) as a function of various anions. Inset of (a) show the visual color changes.
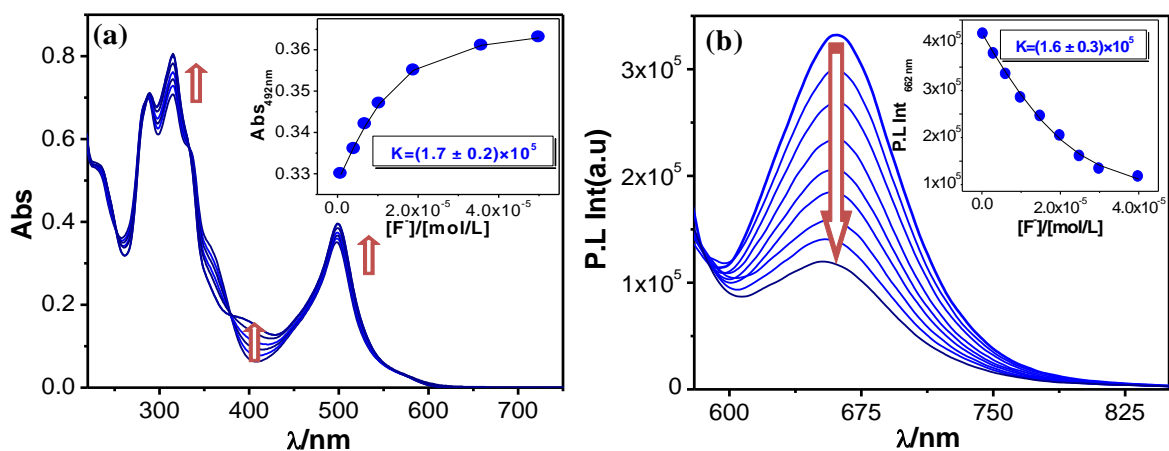
Fig. S16 Change in UV-vis absorption (a) and luminescence (b) spectrum of **1** in MeCN upon incremental addition of F⁻. Insets display the fit of the experimental data to a 1:1 binding profile.
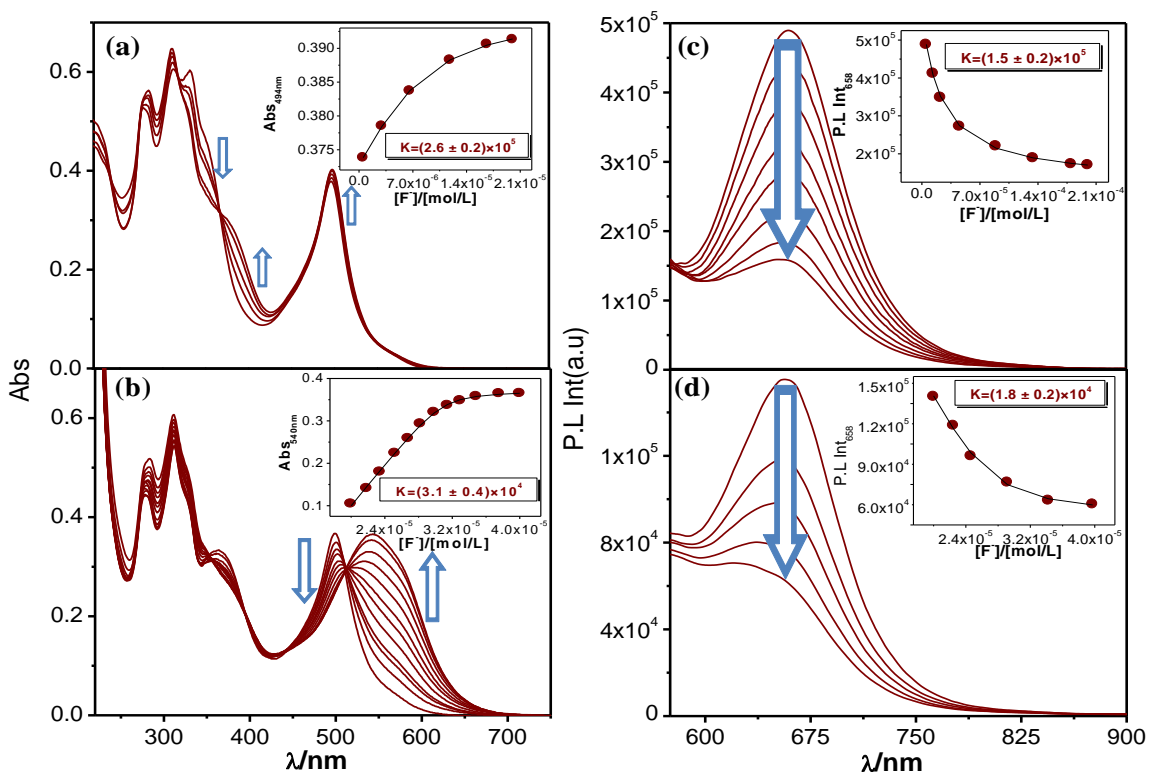
Fig. S17 Absorption and emission spectral change of **2** in MeCN within 0-2 equiv (a and c, respectively) and within 2-4 equiv of F⁻ (b and d, respectively). Insets show the fitting profile of the absorbance and emission spectral data along with its 1:1 binding constant.
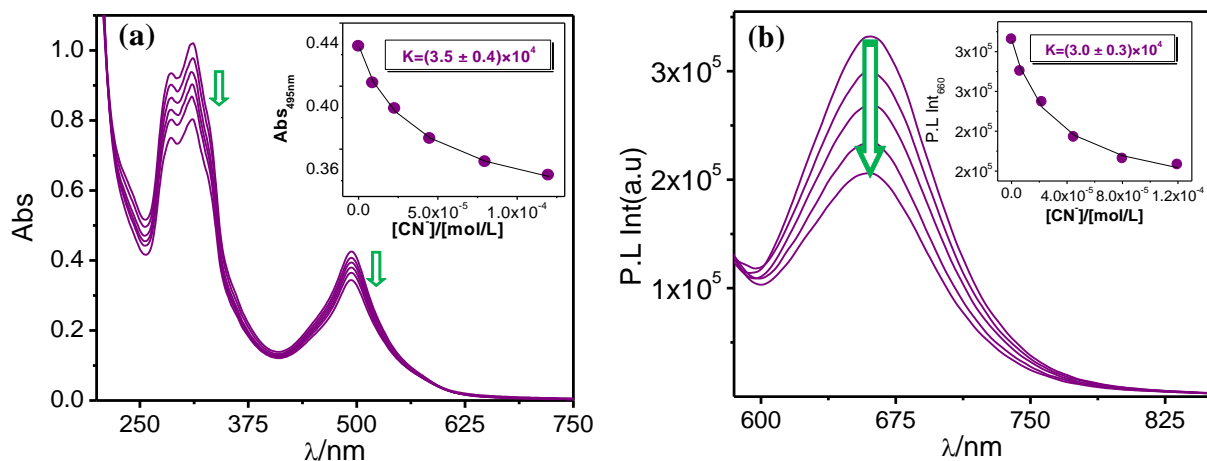
Fig. S18 Change in UV-vis absorption (a) and luminescence (b) spectrum of **1** in water-HEPES buffer (pH = 7.4) upon incremental addition of CN⁻. Insets show the fit of the experimental data to a 1:1 binding profile.
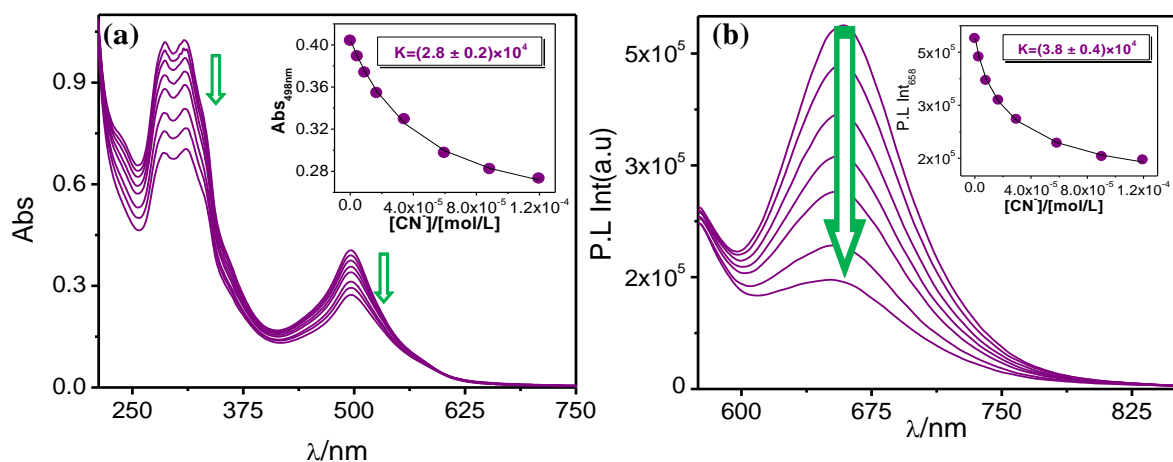
Fig. S19 Change in UV-vis absorption (a) and luminescence (b) spectrum of **2** in water-HEPES buffer (pH = 7.4) upon incremental addition of CN⁻. Insets show the fit of the experimental data to a 1:1 binding profile.
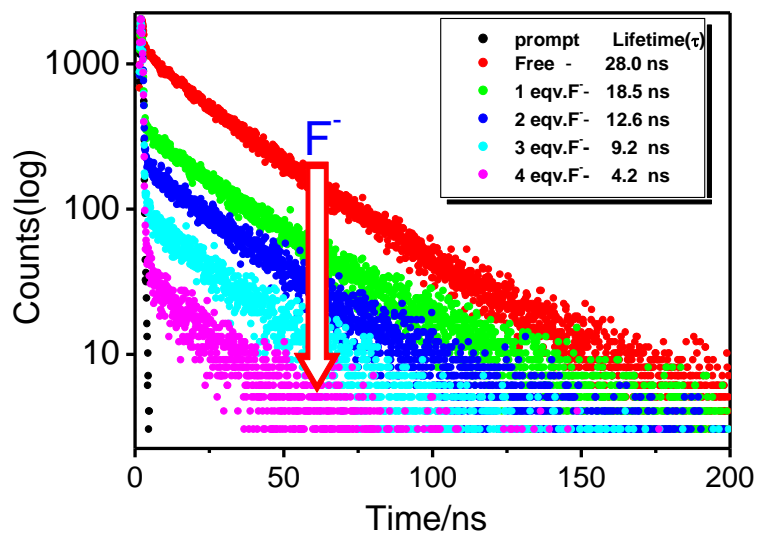
Fig. S20 Change of excited state decay profile of **3** with the variation of F$^-$ in MeCN medium. Inset shows the value of lifetime in presence of different equivalent of F$^-$ added.
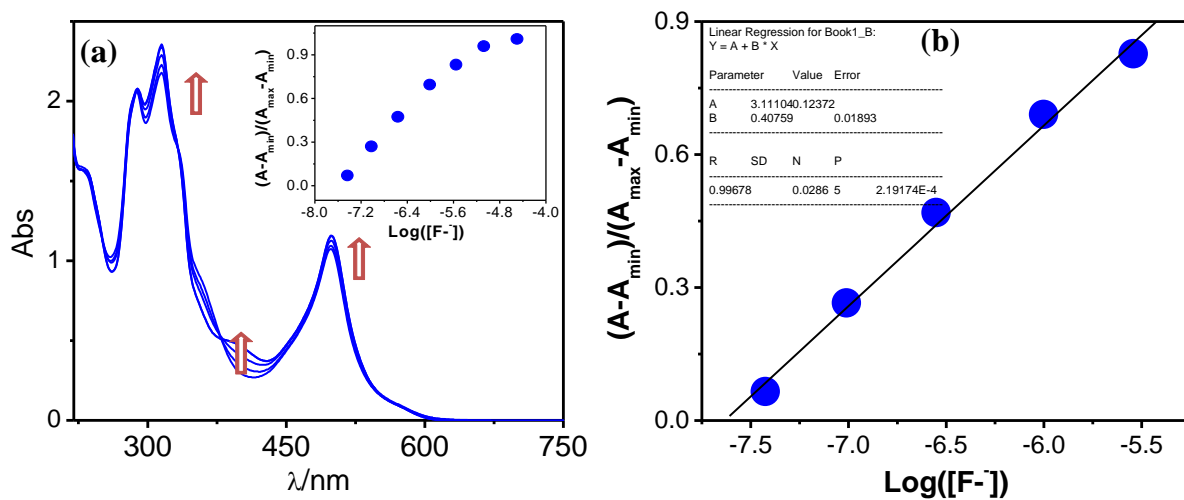
Fig. S21 (a) Absorption spectral changes during the titration of the receptor **1** (1.0×10^{-5} M) with F$^-$ in MeCN, inset: Normalized absorbance between the minimum absorbance and the maximum absorbance. (b) A plot of $(A-A_{min})/(A_{max}-A_{min})$ vs. Log ([F$^-$]), the calculated detection limit of receptor is 2.3×10^{-8} M.
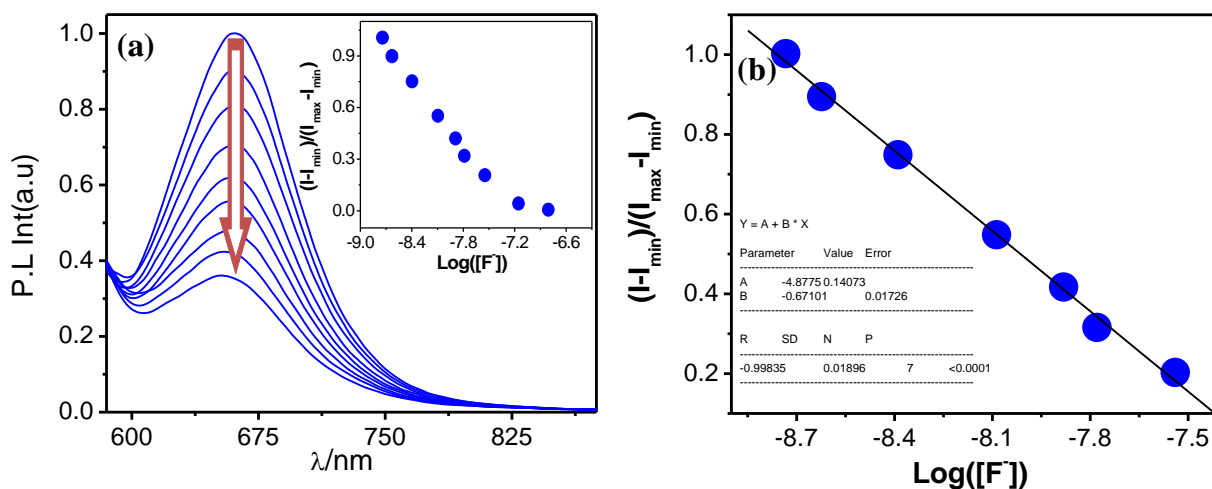
Fig. S22 (a) Emission spectral changes during the titration of the receptor **1** (1.0×10^{-5} M) with F⁻ in MeCN, inset: Normalized intensity between the minimum intensity and the maximum intensity. (b) A plot of $(I-I_{min})/(I_{max}-I_{min})$ vs Log ([F⁻]), the calculated detection limit of receptor is 4.0×10^{-8} M.
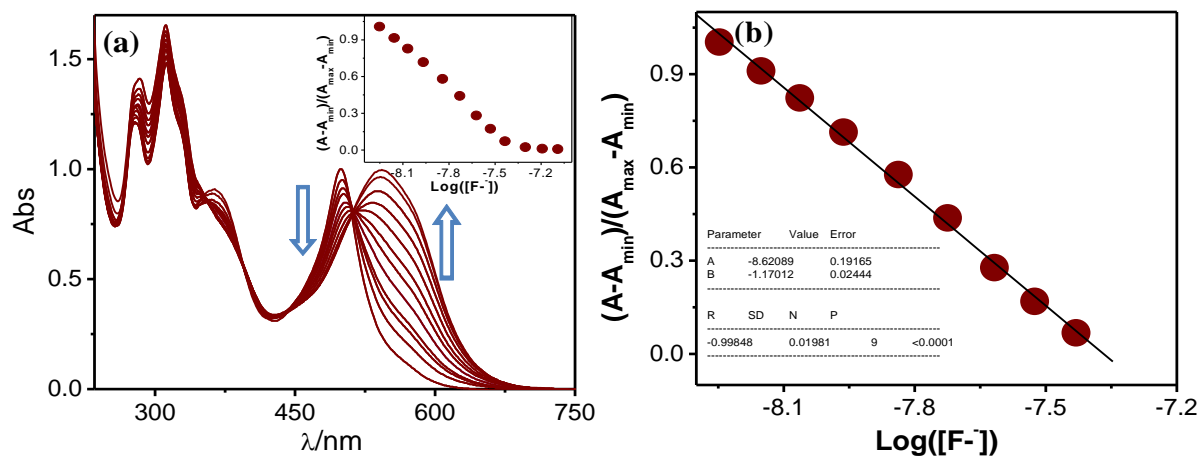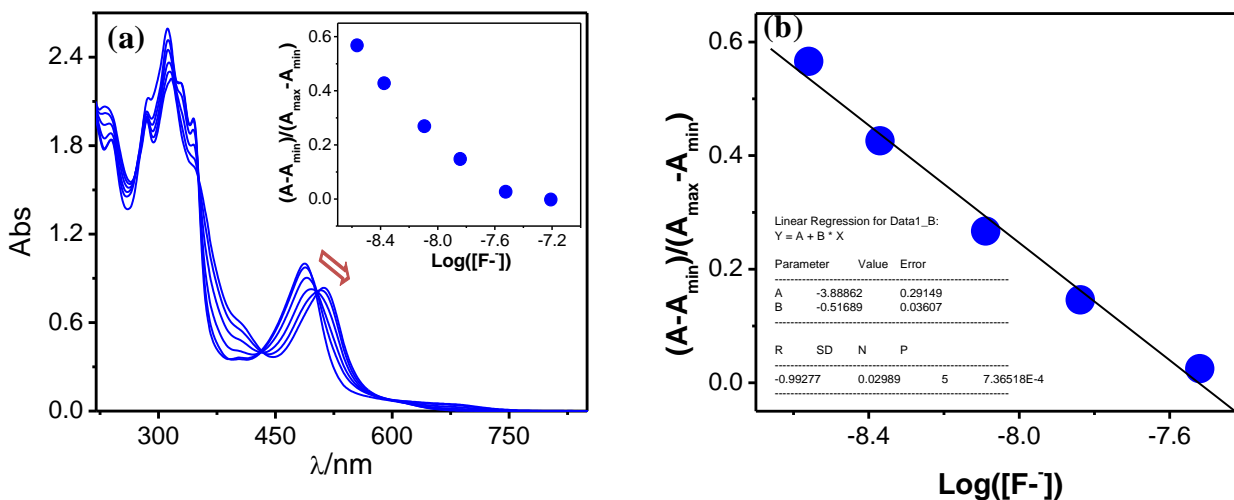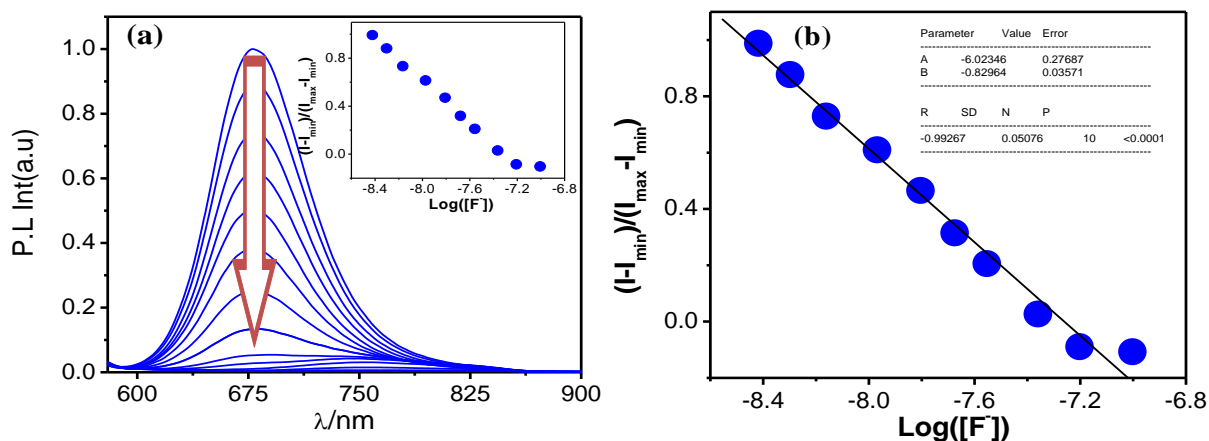

Fig. S23 (a) Absorption spectral changes during the titration of the receptor **2** (1.0×10^{-5} M) with F⁻ in MeCN, inset: Normalized absorbance between the minimum absorbance and the maximum absorbance. (b) A plot of $(A-A_{min})/(A_{max}-A_{min})$ vs. Log ([F⁻]), the calculated detection limit of receptor is 6.3×10^{-8} M.
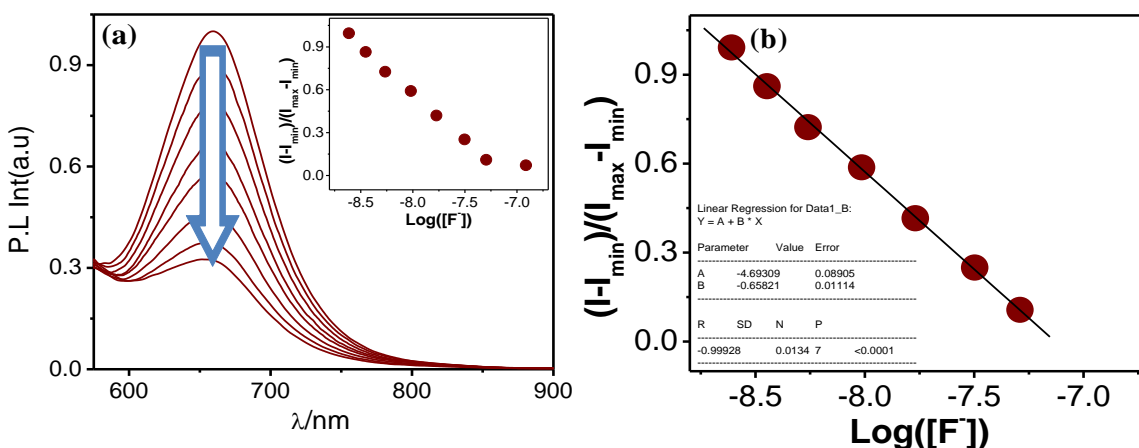
Fig. S24 (a) Emission spectral changes during the titration of the receptor **2** (1.0×10^{-5} M) with F$^-$ in MeCN, inset: Normalized intensity between the minimum intensity and the maximum intensity. (b) A plot of $(I-I_{min})/(I_{max}-I_{min})$ vs Log ([F$^-$]), the calculated detection limit of receptor is 8.0×10^{-8} M.
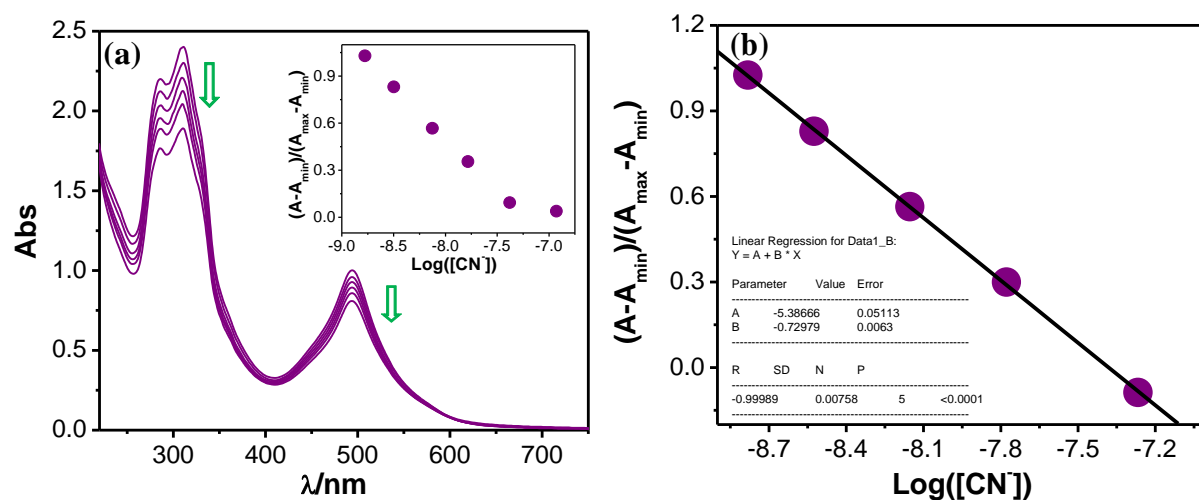

Fig. S25 (a) Absorption spectral changes during the titration of the receptor **3** (1.0×10^{-5} M) with F$^-$ in MeCN, inset: Normalized absorbance between the minimum absorbance and the maximum absorbance. (b) A plot of $(A-A_{min})/(A_{max}-A_{min})$ vs. Log ([F$^-$]), the calculated detection limit of receptor is 4.0×10^{-8} M.
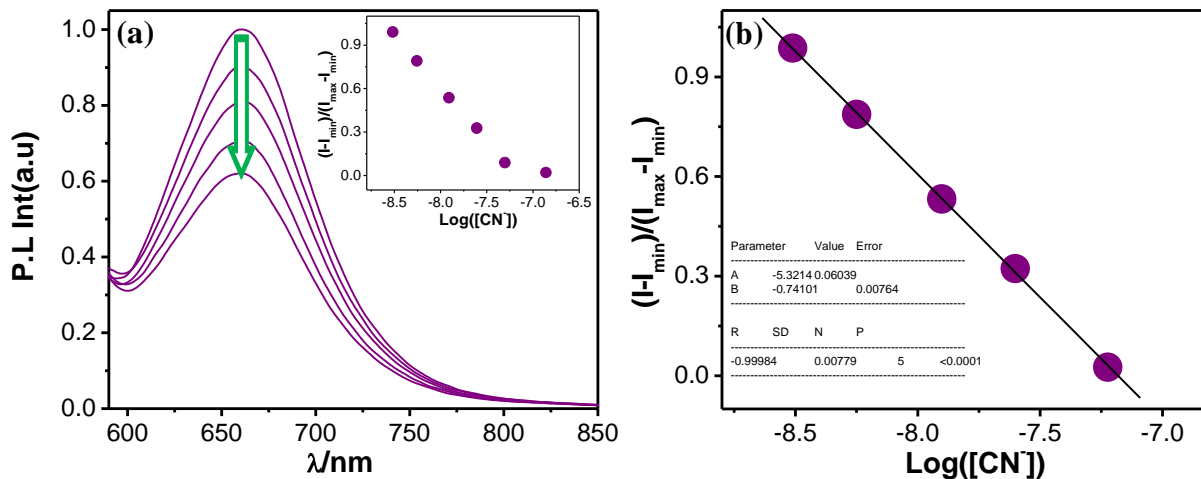
Fig. S26 (a) Emission spectral changes during the titration of the receptor **3** (1.0×10^{-5} M) with F⁻ in MeCN, inset: Normalized intensity between the minimum intensity and the maximum intensity. (b) A plot of $(I-I_{min})/(I_{max}-I_{min})$ vs Log ([F⁻]), the calculated detection limit of receptor is 9.5×10^{-8} M.
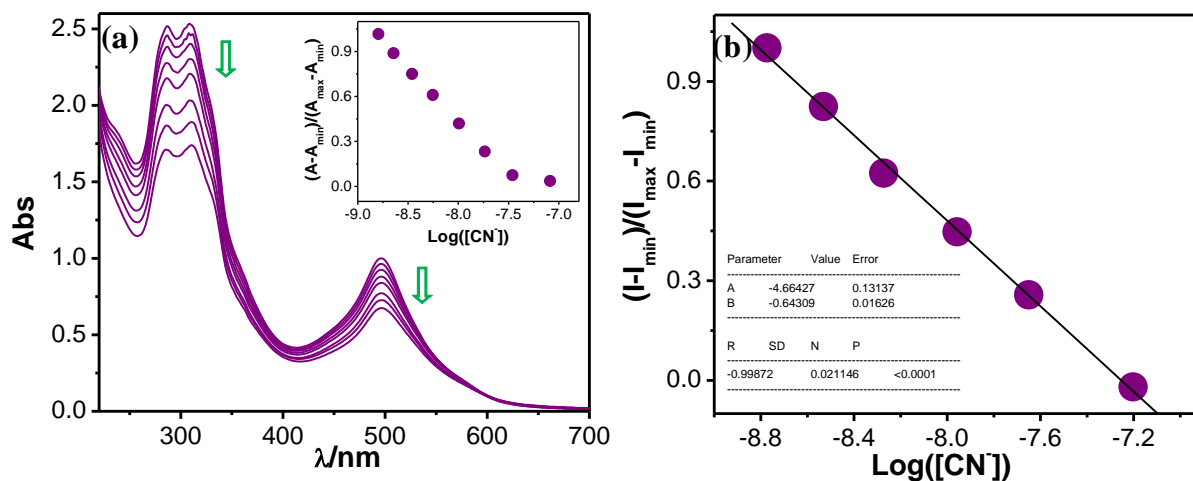

Fig. S27 (a) Absorption spectral changes during the titration of the receptor **1** (1.0×10^{-5} M) with CN⁻ water-HEPES buffer (pH = 7.4), inset: Normalized absorbance between the minimum absorbance and the maximum absorbance. (b) A plot of $(A-A_{min})/(A_{max}-A_{min})$ vs. Log ([CN⁻]), the calculated detection limit of receptor is 7.5×10^{-8} M.
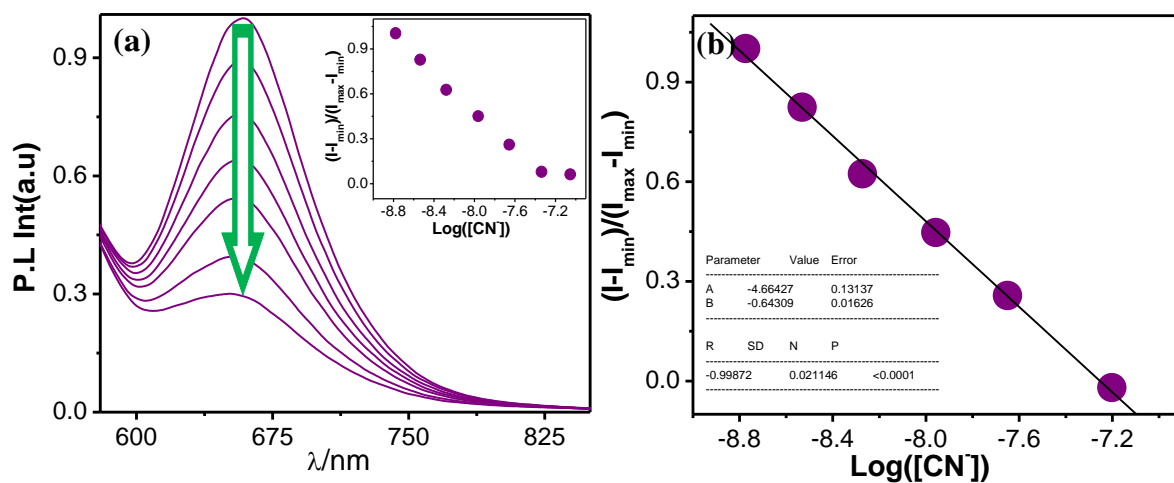
Fig. S28 (a) Emission spectral changes during the titration of the receptor **1** (1.0×10^{-5} M) with CN^- water-HEPES buffer (pH = 7.4), inset: Normalized intensity between the minimum intensity and the maximum intensity. (b) A plot of $(I-I_{min})/(I_{max}-I_{min})$ vs Log ($[CN^-]$), the calculated detection limit of receptor is 7.3×10^{-8} M.
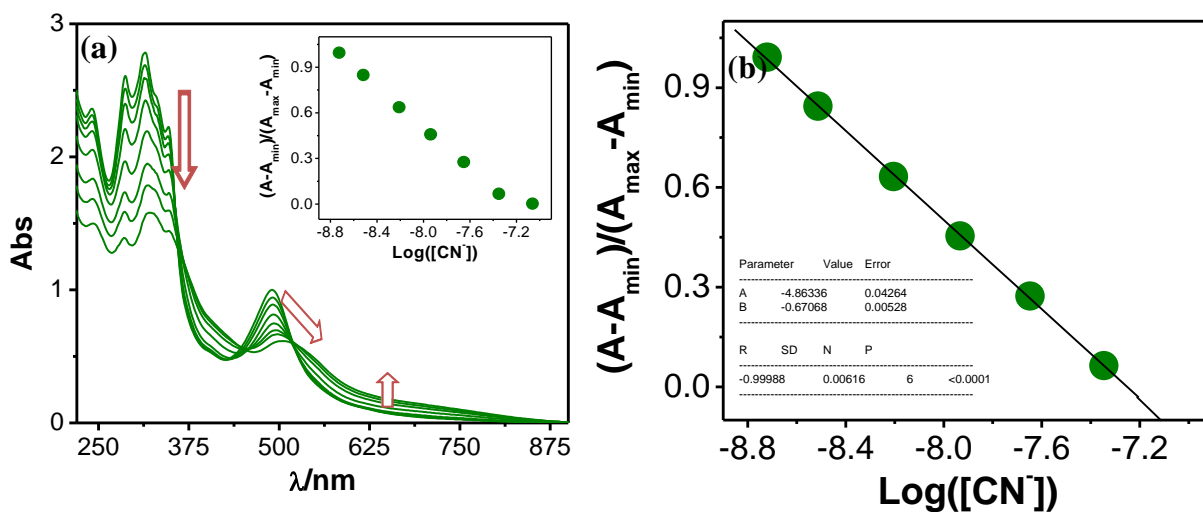

Fig. 29 (a) Absorption spectral changes during the titration of the receptor **2** (1.0×10^{-5} M) with CN^- water-HEPES buffer (pH = 7.4), inset: Normalized absorbance between the minimum absorbance and the maximum absorbance. (b) A plot of $(A-A_{min})/(A_{max}-A_{min})$ vs. Log ($[CN^-]$), the calculated detection limit of receptor is 7.9×10^{-8} M.

Fig. S30 (a) Emission spectral changes during the titration of the receptor **2** (1.0×10^{-5} M) with CN^- water-HEPES buffer (pH = 7.4), inset: Normalized intensity between the minimum intensity and the maximum intensity. (b) A plot of $(I-I_{min})/(I_{max}-I_{min})$ vs Log ($[CN^-]$), the calculated detection limit of receptor is 7.8×10^{-8} M.
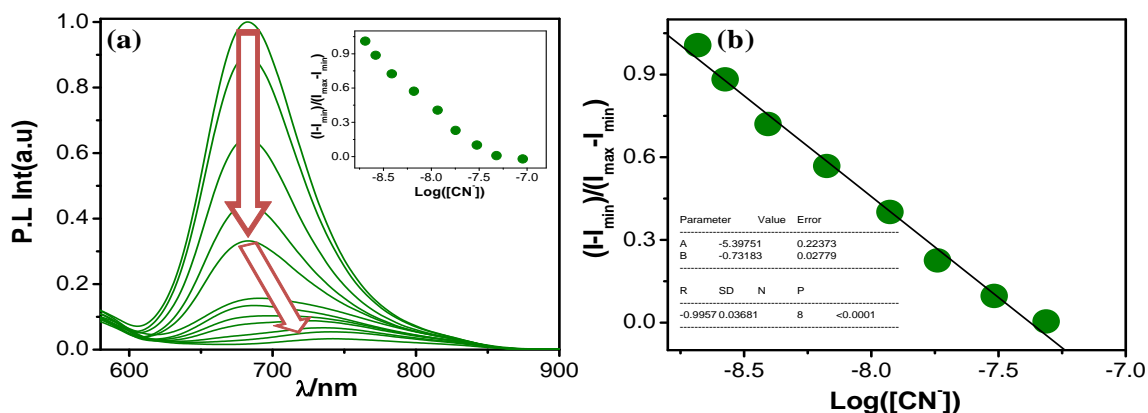

Fig. S31 (a) Absorption spectral changes during the titration of the receptor **3** (1.0×10^{-5} M) with CN^- water-HEPES buffer (pH = 7.4), inset: Normalized absorbance between the minimum absorbance and the maximum absorbance. (b) A plot of $(A-A_{min})/(A_{max}-A_{min})$ vs. Log ($[CN^-]$), the calculated detection limit of receptor is 7.5×10^{-8} M.

Fig. S32 (a) Emission spectral changes during the titration of the receptor **3** (1.0×10^{-5} M) with CN^- water-HEPES buffer (pH = 7.4), inset: Normalized intensity between the minimum intensity and the maximum intensity. (b) A plot of $(I-I_{min})/(I_{max}-I_{min})$ vs Log ($[CN^-]$), the calculated detection limit of receptor is 7.8×10^{-8} M.
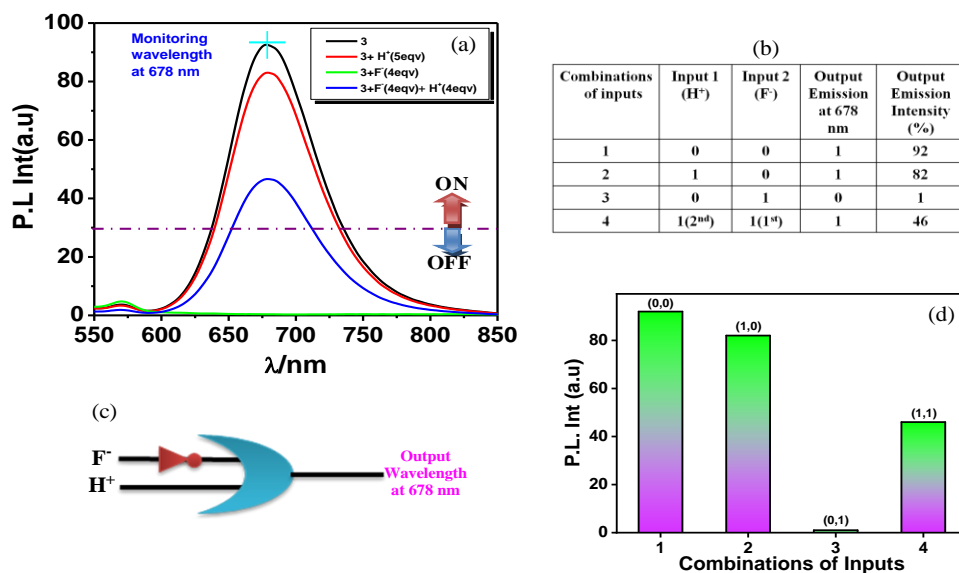

Combinations of inputs	Input 1 (H^+)	Input 2 (F^-)	Output Emission at 678 nm	Output Emission Intensity (%)
1	0	0	1	92
2	1	0	1	82
3	0	1	0	1
4	1(2nd)	1(1st)	1	46

Fig. S33 (a) Emission spectrum of **3** in the presence of H^+ and F^-. (b) Truth table of the IMPLICATION gate. (c) Schematic diagram of this logic system. (d) Histogram of emission intensity in presence of different combinations of inputs.
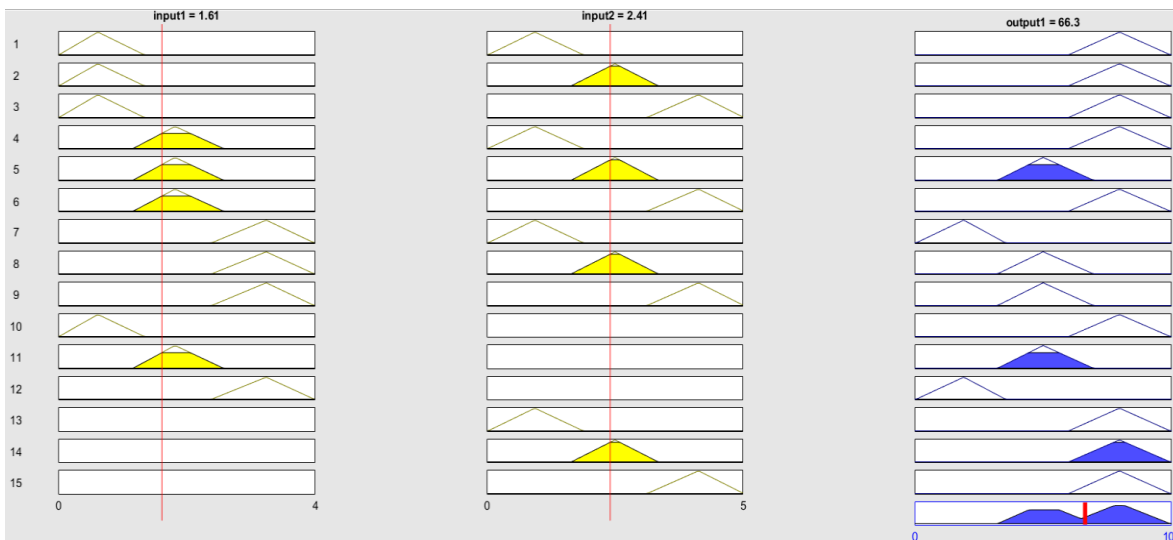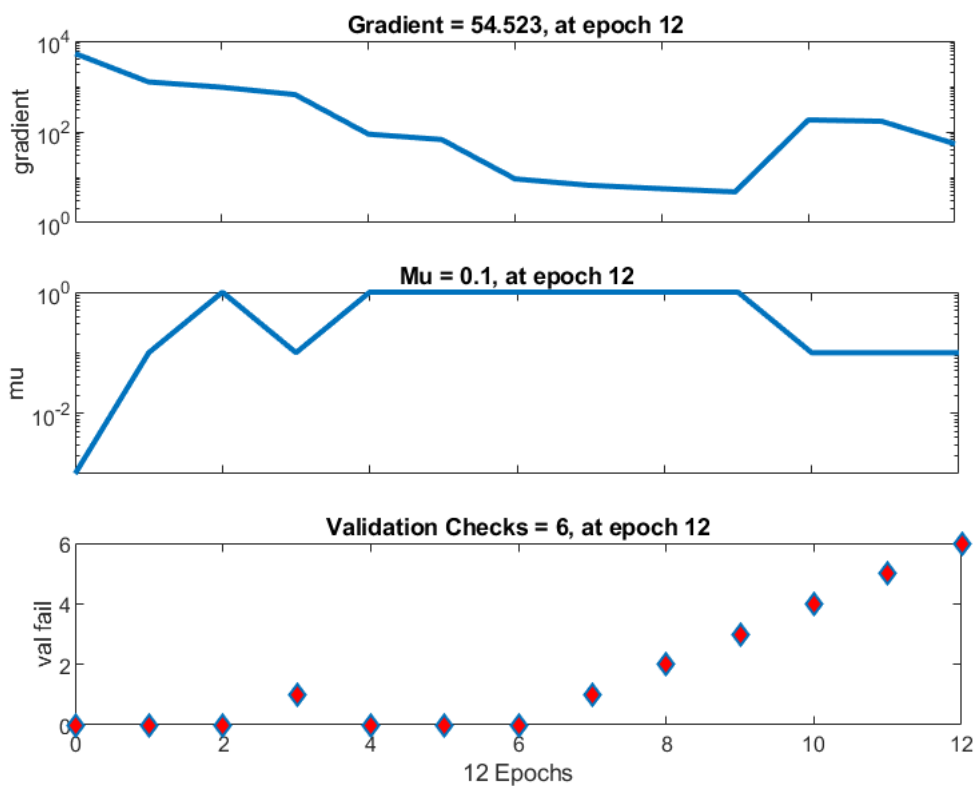
Fig. S34 Mamdani rule view for **3.**

Fig. S35 Training state of the ANN model of **3** (monitoring wavelength at 678nm) up to epoch 12.
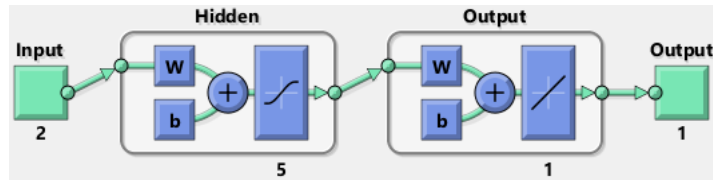
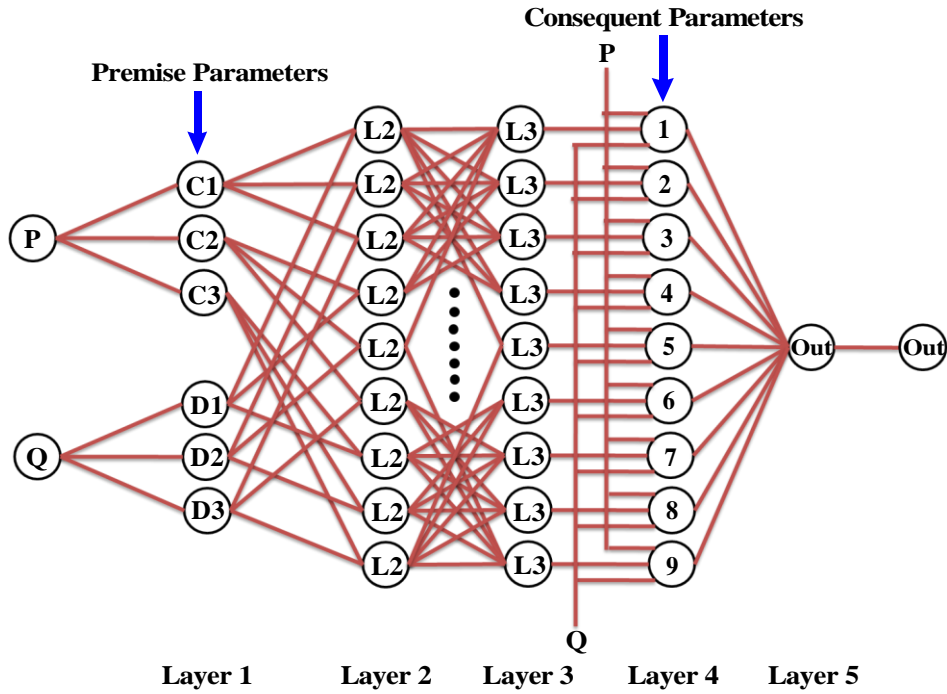**Fig. S36** Artificial neural network model consisting of 2 inputs, 5 hidden layers and 1 output

Fig. S37 Schematic sketch of ANFIS network comprising of two inputs, five layers and one output.
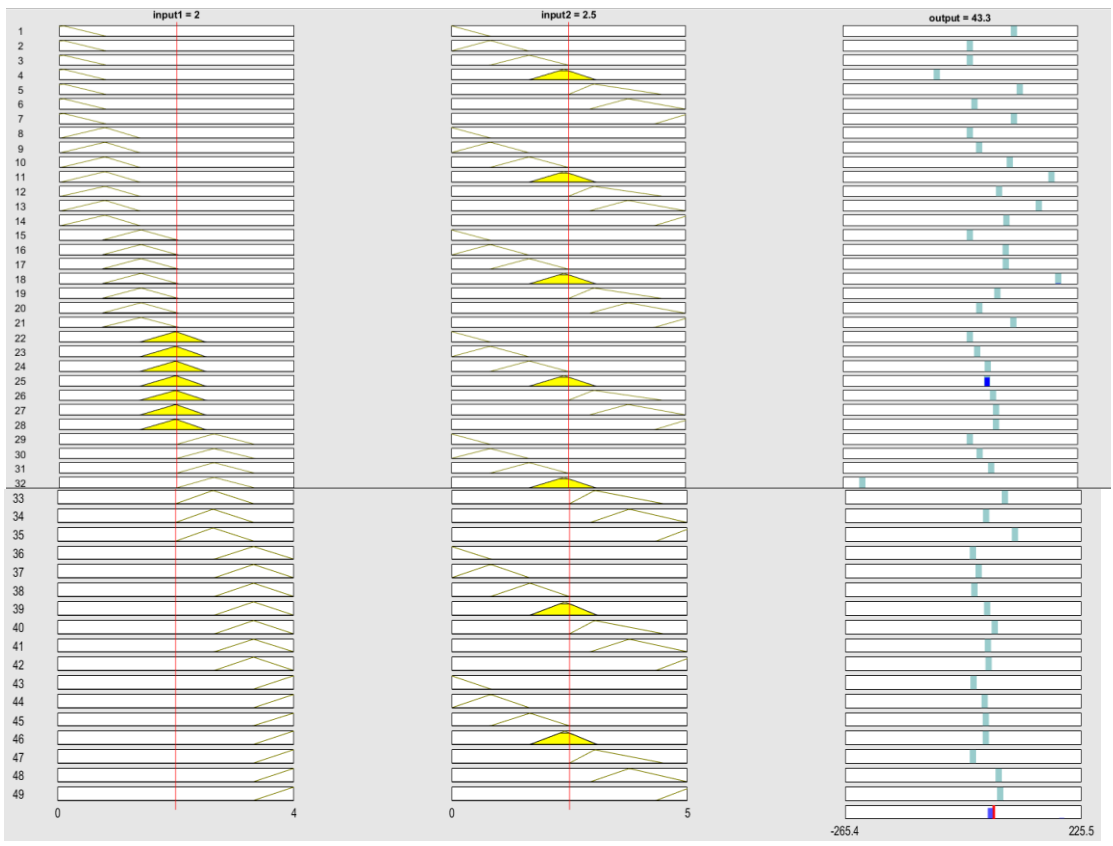
Fig. S38 Sugeno rule view for **3** (monitoring wavelength at 678nm).

Reference

S1.   K. T. Pott, D. A. Usifer, H. D. Abruna, *J. Am. Chem. Soc.* 1987, **109**, 3961-3967.

S2.   M. Haga, T. Takasugi, A. Tomie, M. Ishizuya, T. Yamada, M. Hossain, D.; M. Inoue, *Dalton Trans.* 2003, 2069-2079.

S3.   C. Bhaumik, S. Das, D. Maity, S. Baitalik, *Dalton Trans*. 2012, **41**, 2427-2438.

S4.   S. Deb, A. Sahoo, P. Pal, S. Baitalik, *Inorg. Chem*. 2021, **60**, 6836-6851.

S5.   H. J. Schneider, A. Yatsimirsky, A. Principles and Methods in Supramolecular Chemistry. *John Wiley & Sons, England,* 2000, pp. p.142.

S6.   H. J. Mo, J. J. Wu, Z. P. Qiao, B. H. Ye, Dalton *Trans.,* 2012, **41**, 7026-7036.